INTERNATIONAL JOURNAL OF
NUMERICAL ANALYSIS AND MODELING
Volume 1, Number 1, Pages 1–18

MODELING OF LOW SALINITY EFFECTS IN SANDSTONE OIL ROCKS

ARUOTURE VOKE OMEKEH, STEINAR EVJE, AND HELMER ANDRÉ FRIIS

Abstract. Low salinity water has been reported as being capable of improving oil recovery in sandstone cores under certain conditions. The objective of this paper is the development and examination of a one-dimensional mathematical model for the study of water flooding lab experiments with special focus on the effect of low salinity type of brines for sandstone cores. The main mechanism that is built into the model is a multiple ion exchange (MIE) process, which due to the presence of clay, will have an impact on the water-oil flow functions (relative permeability curves). The chemical water-rock system (MIE process) we consider takes into account desorption and adsorption of calcium, magnesium, and sodium. More precisely, the model is formulated such that the total release of divalent cations (calcium and magnesium) from the rock surface will give rise to a change of the relative permeability functions such that more oil is mobilized. The release of cations depend on several factors like (i) connate water composition; (ii) brine composition for the flooding water; (iii) clay content/capacity. Consequently, the model demonstrates that the oil recovery also, in a nontrivial manner, is sensitive to these factors. An appropriate numerical discretization is employed to solve the resulting system of conservation laws and characteristic features of the model is explored in order to gain more insight into the role played by low salinity flooding waters, and its possible impact on oil recovery.

Key words. low salinity, multiple ion exchange, porous media, two-phase flow, convection-diffusion equations and wettability alteration

1. Introduction

In recent years, brine-rock-oil chemistry has generated a lot of interest in relation to improving oil production from reservoirs. In carbonate reservoirs, the brine constituents have been found to be important for oil recovery [37]. In sandstone reservoirs, the salinity and components of the brine have shown a lot of promise to improve recovery [34, 42, 44]. A number of requirements have been listed as being necessary for low salinity improved recovery. These include:

- Presence of clay [40] or some negatively charged rock surfaces;
- Polar components in the oil phase [35, 40];
- Presence of formation water [40];
- Presence of divalent ion/multicomponent ions in the formation water [24].

Despite meeting the above criteria, some experiments carried out have not shown positive low salinity effect [36, 48]. We also refer to [33] for experimental observations indicating that low salinity water injection as an EOR method appears very sensitive to a combination of several parameters.

1.1. Different mechanisms that have been proposed. Quite a number of different low salinity mechanisms have been put forward in the literature. Some of these mechanisms include:

- *Multicomponent ion exchange (MIE) process* [24]: This mechanism describes the release of oil component previously bonded to the rock surface by divalent ion bridging. Low salinity is said to result in a double layer expansion that makes the desorption of the oil bearing divalent ions from the rock surface possible.
- *pH increase:* The authors of [40] describes a model, in which pH increase as a result of mineral dissolution, is the underlying mechanisms for low salinity induced improved

Received by the editors June 25, 2012 and, in revised form, November 23, 2012.
2000 *Mathematics Subject Classification.* 35R35, 49J40, 60G40.
This research has been supported by the Norwegian Research Council, Statoil, Dong Energy, and GDF Suez, through the project Low Salinity Waterflooding of North Sea Sandstone Reservoirs. The second author is also supported by A/S Norske Shell.

recovery. Austad et al.[6] describe a model of local pH increase as a result of a chemical process involving the release of divalent ions from the rock surface.

- *Clay dispersion[40]:* This mechanism describes a model in which oil-wetted clays are dispersed from the rock surface in low salinity environment. The desorption of divalent ions can only aid such mechanism since divalent ions promotes clay flocculation.

1.2. Main objective of this work. As an attempt to develop some basic understanding of how such mechanisms possibly will have an impact on core flooding experiments in the context of low salinity studies, we will in this work formulate a Buckley-Leverett two-phase flow model where the wetting state, as represented by the relative permeability functions, has been coupled to a multiple ion exchange (MIE) process. In other words, in this work we have singled out MIE as the only mechanisms for taking into consideration possible low salinity effects. More precisely, according to the proposed MIE mechanism, we chose to link desorption of the divalent ions bonded to the rock surface to a change of relative permeability functions such that more oil can be mobilized. This will allow us to do some systematic investigations how different brine compositions can possibly have an impact on the oil recovery.

Hence, the purpose of this work is to, motivated by laboratory experiments with flooding of various seawater like brines, formulate a concrete water-rock chemical system relevant for sandstone flooding experiments with focus on low salinity effects. Main components in the proposed model are:

- Consider modeling of sandstone core plugs with a certain amount of clay attached to it that is responsible for the ion exchange process;
- Include a multiple ion exchange process that involve Ca^{2+}, Mg^{2+}, and Na^{+} ions;
- Implement a coupling between release of divalent ions (calcium and magnesium) from the rock surface and a corresponding change of water-oil flow functions (relative permeability curves) such that more oil can be mobilized.

The resulting model takes the form of a system of convection-diffusion equations:

$$
\begin{aligned}
s_t + f(s,\beta_{ca},\beta_{mg})_x &= 0,\\
(sC_{na} + M_c\beta_{na})_t + (C_{na}f(s,\beta_{ca},\beta_{mg}))_x &= (D(s,\phi)C_{na,x})_x,\\
(sC_{cl})_t + (C_{cl}f(s,\beta_{ca},\beta_{mg}))_x &= (D(s,\phi)C_{cl,x})_x,\\
(sC_{ca} + M_c\beta_{ca})_t + (C_{ca}f(s,\beta_{ca},\beta_{mg}))_x &= (D(s,\phi)C_{ca,x})_x,\\
(sC_{so})_t + (C_{so}f(s,\beta_{ca},\beta_{mg}))_x &= (D(s,\phi)C_{so,x})_x,\\
(sC_{mg} + M_c\beta_{mg})_t + (C_{mg}f(s,\beta_{ca},\beta_{mg}))_x &= (D(s,\phi)C_{mg,x})_x.
\end{aligned}
\tag{1}
$$

For completeness, since we are interested in flooding of seawater like brines (high salinity and low salinity), we have included chloride C_{cl} and sulphate C_{so}, despite that these will act only as tracers in our system. In other words, these ions are not directly involved in the water-rock chemistry model in terms of the MIE process. The unknown variables we solve for are water saturation s (dimensionless), and concentrations C_{na}, C_{cl}, C_{ca}, C_{so}, C_{mg} (in terms of mole per liter water). β_{na}, β_{ca}, and β_{mg} are the concentrations of sodium, calcium, and magnesium bonded to the rock surface. Note that $\beta_i = \beta_i(C_{na}, C_{ca}, C_{mg})$, for $i = na, ca, mg$. Moreover, $f(s,\beta_{ca},\beta_{mg})$ is the fractional flow function. The dependence on β_{ca} and β_{mg} is due to the proposed coupling between wettability alteration and desorption of the divalent cations Ca^{2+} and Mg^{2+} from the rock surface. The quantity M_c represents the mass of clay whereas $D = D(\phi, s)$ is the diffusion coefficient which accounts for both molecular diffusion and mechanical dispersion. More details leading to this model are given in the subsequent sections. In the model (1), a characteristic time $\tau = \frac{\phi L}{v_T}$ and length scale L have been introduced.

Such a model can potentially be a helpful tool for visualizing in a systematic manner the relatively complicated interplay between (i) change in injecting brine compositions; (ii) change in formation water compositions; (iii) clay content/capacity. This can also serve as a help to design new laboratory experiments. In particular, we observe a number of different scenarios:

- Certain low salinity brines can give rise to adsorption of both Ca^{2+} and Mg^{2+} ions. This will give no additional oil recovery due to the fact that the model predicts no change in the wetting state.
- Other low salinity brines give rise to desorption of both Ca^{2+} and Mg^{2+} ions. This will give favorable results as far as the oil recovery is concerned.
- Seawater type of brines may show adsorption of Mg^{2+} ions and desorption of Ca^{2+} ions. This will in turn give oil recovery curves that sometimes are different from those obtained by using the low salinity brines.
- Whether desorption or adsorption of divalent ions will take place is also a result of the formation brine composition relative to the injecting brine composition.

We remark that capillary pressure is being neglected in this paper. Depending on the flow velocity and the particular capillary pressure curves, capillary pressure effects might be significant on the core scale. In addition the so-called capillary end effect will always be present when laboratory coreflood experiments are performed. We also mention that the capillary pressure might be affected by wettability changes as studied in this work. However, as emphasized above our main intention is to obtain a basic understanding of the proposed flow model with the MIE process as a low salinity mechanism. For that purpose it is preferable to keep the mathematical model as simple as possible, in order to avoid unnecessary complications in the interpretation of the model behavior. Moreover, capillary pressure is not expected to influence the ion exchange to a large extent. This process is affected mainly by the ion concentrations, clay content and selectivity. Our results will thus essentially cover laboratory behavior that is relevant for a larger scale where capillary pressure often plays a minor role. Effects of including capillary pressure as well as mineral solubility in the present mathematical model will be explored in a future paper.

1.3. Other works. A lot of work on low salinity have been published in the literature. We group them under experimental and modeling works. While a lot of experimental work have been published, relatively few modeling works can be found. The authors of [21] and [44] carried out standard waterflood with Moutray crude oil and Berea sandstone to show the effect of brine composition on oil recovery. Their work showed that ageing and flooding with $CaCl_2$ based brine gave more recovery than NaCl brine. Sharma and Filoco [35] studied the effect of salinity on recovery of Berea sandstone cores with crude oil and NaCl brines. Beneficial low salinity effect was reported when both the connate and the invading brine was of the same salinity, but no effect was seen when the invading brine was of lower salinity than the connate brine or when refined crude was used.

The authors of [5],[39] and [48] performed secondary waterflood experiments (i.e., injected brine different from connate brine) with Berea sandstone. Tang and Morrow [39] reported beneficial effect with injection of low salinity water independent of the valency of the invading brine. Zhang and Morrow [48] used three groups of Berea sandstone (60md, 500md and 1100md) and reported no tangible low salinity effect in the 60md and 1100md cores. Ashraf et. al [5] studied the low salinity effect at different wetting conditions by using different oil with different wetting conditions with the Berea sandstone and connate brine. Ashraf et. al [5] reported different degrees of low salinity success with each wetting condition; a water wetting state was reported to perform best.

Alotaibi et al. [3],Boussour et al. [33], Cissokho et al.[13], Pu et al. [31] and Skrettingland et al. [36] carried out tertiary waterflood experiments. This involves injecting with the connate brine before changing to a different invading brine at a high water cut after breakthrough, usually when no more oil is produced with the connate brine. Alotaibi et al. [3] flooded with Berea core and reported mixed result with low salinity injection, depending on the water-rock interaction. Cissokho et al. [13] used an outcrop sandstone core with another clay type apart from kaolinite and reported improved low salinity recovery. Skrettingland et al. [36] used north-sea reservoir cores and reported very minor response to low salinity at both high pressure and low pressure floods. Pu et al. [31] used a reservoir core with almost no clay content but with substantial amount of dolomite crystal and reported low salinity response in spite of the near absence of clay.

Finally, Webb et al. [43] determined the water-oil relative permeability curves of high and low salinity water using cores from different sandstone reservoirs and performed the experiments

under full reservoir conditions. In particular, different water-oil relative permeability curves for high and low salinity water was reported. Berg et al. [9] devised an experiment where they were able to film the release of oil droplets bonded to clay layers when the clay layers were exposed to low salinity water in a flow cell. The authors attributed this release of oil droplets to either double layer expansion or cation exchange.

The above review deals with experimental related works. We now mention some of the modeling related work we are aware of which seems relevant for low salinity flooding experiments. The authors of [22], [41] and [47] modeled beneficial low salinity effects by directly linking the brine salinity to the flow conditions (relative permeability and/or capillary pressure). Using this principle, Tripathi et al. [41] studied flow instability at the saturation fronts. Jerauld et al. [22] studied the dispersion at the saturation front. Yu-shu and Baojun [47] included the possible adsorption/desorption of salt but did not link the adsorbed salt to improved flow functions. Two highly interesting works, in view of the proposed model (1), are represented by [38] and [29]. They studied a general system of the form

$$\begin{aligned} s_t + f(s,\mathbf{c})_x &= 0, \\ (\mathbf{c}s + \mathbf{a}(\mathbf{c}))_t + (\mathbf{c}f(s,\mathbf{c}))_x &= 0, \end{aligned} \tag{2}$$

for n components $\mathbf{c} = (c_1, \ldots, c_n)$. If diffusion effects are ignored in model (1), it can be considered as a special case of (2). The authors of [38] and [29] introduced a reformulation of the model by employing a coordinate transformation which decouples the hydrodynamic part from the thermodynamic. Hence, they could produce analytical solutions for various problems. Such techniques could most likely be used for our model to allow for fast calculations. However, it is beyond the scope of this work since the main objective here is to obtain a model which can be used to test various hypothesis for how low salinity effects may impact the oil recovery. We would also mention that the model (1) is a generalization of the one studied in [45, 46] in the sense that in those works only adsorption of a single component is considered, not a multiple ion exchange process involving several components.

Finally, the model we are presenting in this paper has been used in [28] to explain the behavior observed in some low salinity waterflood experiments where expected low salinity improved recovery were not seen.

1.4. Structure of paper. The rest of this paper is organized as follows: In Section 2 we mathematically describe the multiple ion exchange process built into the flow model. In Section 3 we explain how the MIE process is linked to a change of the wetting state as represented by two sets of relative permeability functions referred to as high salinity and low salinity conditions. Section 4 gives a presentation of the flow equations where the two-phase flow and ion concentration flow dynamics are accounted for. In Section 5 some details are given of the numerical approach used to solve the coupled system (1). Finally, Section 6 presents a number of different flow cases whose purpose is to illustrate basic features of the model as a tool to explore the relation between the behavior of the MIE process and oil recovery curves.

2. Modeling of the multiple ion exchange (MIE) process

In this section we describe the multiple ion exchange process we shall rely on in this work.

2.1. Generally. We distinguish between concentration C and chemical activity a noting that they are related by

$$a = \gamma C, \tag{3}$$

where γ is the activity coefficient. According to the extended Debuye-Hückel equation, see for example [4, 25] and [27] (page 25), the activity coefficient γ_i is given by

$$\log_{10}(\gamma_i) = \frac{-AZ_i^2\sqrt{I_0}}{1 + a_i^0 B\sqrt{I_0}} + bI_0, \tag{4}$$

where the index i refers to the different species involved in the system which is studied. Moreover, Z_i refers to the ionic charges, b is an extended term parameter, $A(T)$ and $B(T)$ are temperature

dependent given functions [4, 19], similarly for the constants a_i^0, whereas I_0 refers to the ionic strength defined by

$$I_0 = \frac{1}{2}\sum_i C_i Z_i^2. \tag{5}$$

For the numerical calculations, we calculate I_0 in each grid block based on the ion concentrations for the previous time step. Consequently, I_0 is always updated throughout the flooding process. Hence the activity coefficients are updated as well, according to equation (4).

2.2. Cation exchange. The cation exchange model include the following ions: Na^+, Ca^{2+} and Mg^{2+}. Though the proton (H^+) ion has a stronger displacing power, its concentration in oil reservoirs is considered to be low in comparison to the other ions in reservoir condition. Typically the pH of oil reservoirs fall in the range between 5-7 fixing the H^+ concentrations at between 10^{-5} to 10^{-7} which is low compared to the other cation concentrations (see Tables 1, 2, 3 and 4). For this reason we expect that the H^+ concentration on the clay surface to be negligible compared to the other cations and we have chosen not to include it in the ion exchange reactions.

We model the cation exchange using the Gapon model.

$$\begin{aligned} \frac{1}{2}Ca^{2+} + \text{Na-X} &\rightleftharpoons \text{Ca}_{\frac{1}{2}}\text{-X} + Na^+, \\ \frac{1}{2}Mg^{2+} + \text{Na-X} &\rightleftharpoons \text{Mg}_{\frac{1}{2}}\text{-X} + Na^+. \end{aligned} \tag{6}$$

This model has been used in the modeling of cation exchange in chemical flooding [30]. The Gapon model is based on a single monovalent exchange site and as such makes no difference on the choice of unit for the activity of the absorbed ion [4]. The model can also be expressed as an equivalent of the Langmuir multicomponent isotherm as done in equations (11), (12) and (13). There have been concerns about the performance of the model when several heterovalent ions are present. However it is popular among soil scientists and has been used extensively to model irrigation systems containing Na^+, Ca^{2+} and Mg^{2+} [4].

Other popular ion exchange models make use of the number of exchangeable cations convention and the reaction written thus

$$\begin{aligned} \frac{1}{2}Ca^{2+} + \text{Na-X} &\rightleftharpoons \frac{1}{2}\text{Ca-X}_2 + Na^+, \\ \frac{1}{2}Mg^{2+} + \text{Na-X} &\rightleftharpoons \frac{1}{2}\text{Mg-X}_2 + Na^+. \end{aligned} \tag{7}$$

Expressing the exchange reactions as done in (7) makes the choice of the unit for the activity of the absorbed specie important. The Gaines–Thomas model uses equivalents as units of the absorbed specie. The use of molar units for the absorbed species follows the Kerr or Vanslow convention.

The exchange reactions are supposed to take place at a fast rate. Constant selectivity factors K_{cana} and K_{mgna} are assumed, and using the Gapon model (6) they are expressed as

$$K_{cana} = \frac{\beta_{ca}\gamma_{na}C_{na}}{\beta_{na}\sqrt{\gamma_{ca}C_{ca}}}, \tag{8}$$

$$K_{mgna} = \frac{\beta_{mg}\gamma_{na}C_{na}}{\beta_{na}\sqrt{\gamma_{mg}C_{mg}}}, \tag{9}$$

and

$$\beta_{na} + 2\beta_{mg} + 2\beta_{ca} = CEC, \tag{10}$$

where β_{na}, β_{mg} and β_{ca} are the number of moles of Na^+, Mg^{2+} and Ca^{2+} ions attached to a unit mass of clay. The CEC as used here is the Cation Exchange Capacity in equivalent/Kg. The equation system (8), (9) and (10) is linear in the variables β_{na}, β_{mg} and β_{ca}, and a solution can easily be obtained. We find that

$$\beta_{na}(C_{na}, C_{ca}, C_{mg}) = \frac{\gamma_{na}C_{na}CEC}{2K_{cana}\sqrt{\gamma_{ca}C_{ca}} + 2K_{mgna}\sqrt{\gamma_{mg}C_{mg}} + \gamma_{na}C_{na}}, \tag{11}$$

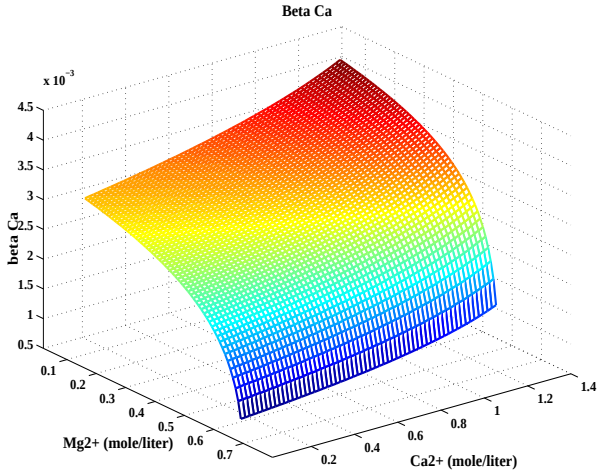

FIGURE 1. Plot showing β_{ca} as a function of varying C_{ca} and C_{mg} concentrations, and with $C_{na} = 0.15$ (moles per liter). Other parameters in (12) like K_{cana}, K_{mgna}, and CEC, are listed in Appendix A.

$$\beta_{ca}(C_{na}, C_{ca}, C_{mg}) = \frac{K_{cana}\sqrt{\gamma_{ca}C_{ca}}CEC}{2K_{cana}\sqrt{\gamma_{ca}C_{ca}} + 2K_{mgna}\sqrt{\gamma_{mg}C_{mg}} + \gamma_{na}C_{na}}, \tag{12}$$

and

$$\beta_{mg}(C_{na}, C_{ca}, C_{mg}) = \frac{K_{mgna}\sqrt{\gamma_{mg}C_{mg}}CEC}{2K_{cana}\sqrt{\gamma_{ca}C_{ca}} + 2K_{mgna}\sqrt{\gamma_{mg}C_{mg}} + \gamma_{na}C_{na}}. \tag{13}$$

We note that the equations (11), (12) and (13) are equivalent to a Langmuir-type adsorption isotherm. Fig. 1 illustrates how the β_{ca} function depends on the concentrations C_{na}, C_{ca}, C_{mg}. At high magnesium concentration, the amount of calcium ion adsorbed on the rock, β_{ca}, becomes quite low.

3. Coupling of wettability alteration to changes on the rock surface

This section discusses aspects concerning the flow functions. Since we only consider flows without capillary pressure in Section 6, we limit the discussion to the relative permeability functions. The following ideas are also employed in [14, 15], however, in the context of spontaneous imbibition on chalk cores where capillary forces are the driving forces in oil recovery. It also partially follows ideas employed in previous works in [22, 41, 45].

3.1. Relative permeability functions. As a basic model for relative permeability functions the well-known Corey type correlations are used [12]. They are given in the form (dimensionless functions)

$$\begin{aligned} k(s) &= k^*\Big(\frac{s - s_{wr}}{1 - s_{or} - s_{wr}}\Big)^{Nk}, \qquad s_{wr} \le s \le 1 - s_{or}, \\ k_o(s) &= k_o^*\Big(\frac{1 - s_{or} - s}{1 - s_{or} - s_{wr}}\Big)^{Nk_o}, \qquad s_{wr} \le s \le 1 - s_{or}, \end{aligned} \tag{14}$$

where s_{wr} and s_{or} represent critical saturation values and Nk and Nk_o are the Corey exponents that must be specified. In addition, k^* and k_o^* are the end point relative permeability values that also must be given. Now, we define two extreme relative permeability functions corresponding to the wetting state of the rock for high salinity and low salinity conditions.

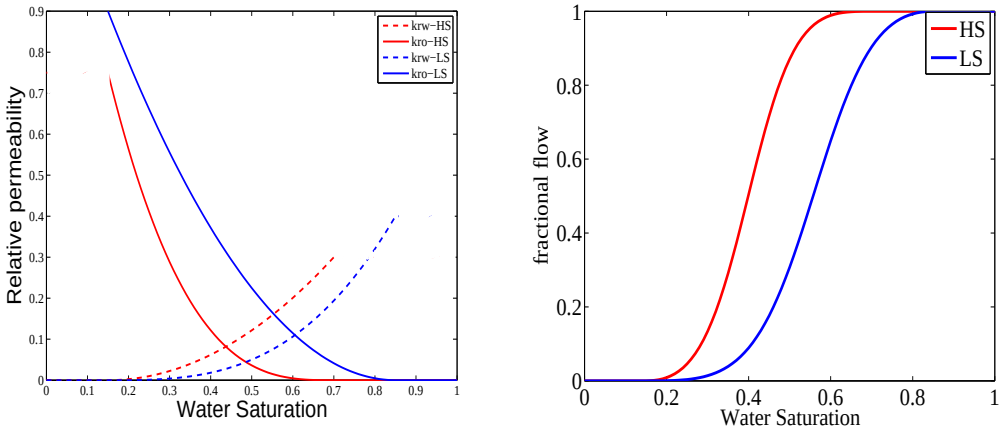

FIGURE 2. **Left**: Example of relative permeability curves corresponding to high-salinity (HS) and low-salinity (LS) conditions. **Right**: Corresponding fractional flow functions.

3.1.1. High salinity conditions. This is assumed to be the initial state of the core. The values for generating the functions are listed in Appendix B. Applying the values of the *high salinity* condition in (14) the following two relative permeability curves are obtained

$$k^{HS}(s; s_{wr}^{HS}, s_{or}^{HS}), \qquad k_o^{HS}(s; s_{wr}^{HS}, s_{or}^{HS}), \qquad \text{for } s_{wr}^{HS} \le s \le 1 - s_{or}^{HS}. \tag{15}$$

We refer to Fig. 2 for a plot of these curves (red line).

3.1.2. Low salinity conditions. This wetting condition is assumed to be attained only when there is complete desorption of Ca^{2+} and Mg^{2+} ions from the rock surface. The values for generating the functions are listed in Appendix B. Applying the values of the *low salinity* condition in (14) gives corresponding relative permeability curves

$$k^{LS}(s; s_{wr}^{LS}, s_{or}^{LS}), \quad k_o^{LS}(s; s_{wr}^{LS}, s_{or}^{LS}), \quad \text{for } s_{wr}^{LS} \le s \le 1 - s_{or}^{LS}. \tag{16}$$

We refer to Fig. 2 for a plot of these curves (blue line). The motivation for the choice of the values was to match the form of the relative permeability measured for a variety of high salinity and low salinity brines in [43].

3.2. Cation exchange as a mechanism for wettability alteration. We let β_{ca0} and β_{mg0} be the amount of calcium and magnesium, respectively, initially bounded to the clay surface. We then define the quantity

$$m(\beta_{ca}, \beta_{mg}) := \max(\beta_{ca0} - \beta_{ca}, 0) + \max(\beta_{mg0} - \beta_{mg}, 0), \tag{17}$$

as a measure for the desorption of cations from the clay. Moreover, we define

$$H(\beta_{ca}, \beta_{mg}) := \frac{1}{1 + rm(\beta_{ca}, \beta_{mg})}, \tag{18}$$

where $r > 0$ is a specified constant. Note that the choice of r determines the extent in which the divalent ion desorbed leads to a certain change of the wetting state.

The function $H(\beta_{ca}, \beta_{mg})$ is a weighting function, and works such that $H = 1$, when there is no desorption of calcium and magnesium from the rock, whereas $0 < H < 1$ in case of desorption of at least one of these cations. How fast $H(\beta_{ca}, \beta_{mg})$ is approaching 0 as $m(\beta_{ca}, \beta_{mg})$ is increasing, depends on the choice of r. Now, the weighting function $H(\beta_{ca}, \beta_{mg})$ can be used to represent the wetting state in the core plug; $H(\beta_{ca}, \beta_{mg}) = 1$ corresponds to the initial oil-wet state, whereas $H(\beta_{ca}, \beta_{mg}) \approx 0$ represents the water-wet state. By defining relative permeability curves by means of the weighting function $H(\beta_{ca}, \beta_{mg})$ as described in the next subsection, the model can account

for a dynamic change from an initial high salinity state towards a low salinity state controlled by the degree of desorption of calcium and magnesium from the core.

3.3. Modeling of transition from high salinity to low salinity conditions. In this work, we follow along the lines of [14, 15], and model wettability alteration by defining relative permeability curves through an interpolation between the high salinity and low salinity curves given by (14), combined with the data specified in Appendix B as given by (97) and (98).

More precisely, motivated by the proposed hypothesis that transition from a high salinity wetting state towards low salinity conditions depends on the desorption of calcium and magnesium caused by the cation exchange process, the following interpolation is proposed:

$$k(s,\beta_{ca},\beta_{mg}) = H(\beta_{ca},\beta_{mg})k^{HS}(s) + [1 - H(\beta_{ca},\beta_{mg})]k^{LS}(s), \tag{19}$$

where $H(\beta_{ca},\beta_{mg})$ is defined by (18). Hence, when no desorption of divalent cations from the clay surface takes place it follows that $H(\beta_{ca},\beta_{mg}) = 1$, implying that $k(\beta_{ca},\beta_{mg}) = k^{HS}(s)$. This reflects the initial high salinity wetting state. Then, as desorption of divalent cations takes place, it follows that $m(\beta_{ca},\beta_{mg})$ increases. In particular, if the desorption effects becomes large enough, it follows from the above discussion (see equation (18)) that $H(\beta_{ca},\beta_{mg}) \approx 0$, which means that $k(s,\beta_{ca},\beta_{mg}) \approx k^{LS}(s)$, reflecting that a wettability alteration has taken place which results in a low salinity wetting state.

4. The coupled model for water-oil flow and multiple ion exchange

We now want to take into account convective and diffusive forces associated with the brine as well as the oil phase. In order to include such effects we must consider the following equations for the total concentrations ρ_o, ρ_l, ρ_{ca}, ρ_{so}, ρ_{mg}, ρ_{na}, ρ_{cl} (mol per liter core):

$$\begin{aligned}
\partial_t\rho_o + \nabla\cdot(\rho_o\mathbf{v}_o) &= 0, && \text{(oil flowing through the pore space)}\\
\partial_t\rho_l + \nabla\cdot(\rho_l\mathbf{v}_l) &= 0, && \text{(water flowing through the pore space)}\\
\partial_t\rho_{na} + \partial_t(M_c\beta_{na}) + \nabla\cdot(\rho_{na}\mathbf{v}_g) &= 0, && (\mathrm{Na}^+\text{-ions in water})\\
\partial_t\rho_{cl} + \nabla\cdot(\rho_{cl}\mathbf{v}_g) &= 0, && (\mathrm{Cl}^-\text{-ions in water})\\
\partial_t\rho_{ca} + \partial_t(M_c\beta_{ca}) + \nabla\cdot(\rho_{ca}\mathbf{v}_g) &= 0, && (\mathrm{Ca}^{2+}\text{-ions in water})\\
\partial_t\rho_{so} + \nabla\cdot(\rho_{so}\mathbf{v}_g) &= 0, && (\mathrm{SO}_4^{2-}\text{-ions in water})\\
\partial_t\rho_{mg} + \partial_t(M_c\beta_{mg}) + \nabla\cdot(\rho_{mg}\mathbf{v}_g) &= 0, && (\mathrm{Mg}^{2+}\text{-ions in water}).
\end{aligned} \tag{20}$$

Here $\mathbf{v}_o$, $\mathbf{v}_l$ and $\mathbf{v}_g$ are, respectively, the oil, water and species "fluid" velocities, whereas M_c represents the mass of the clay. The subsequent derivation of the model closely follows the work [14, 15], however, the water-rock chemistry in our current model is given in terms of a multiple ion exchange process (MIE), not dissolution/precipitation as in [14, 15].

Let s_o denote the oil saturation, i.e. the fraction of volume of the pore space represented by porosity ϕ that is occupied by the oil phase, and s the corresponding water saturation. The two saturations are related by the basic relation $s_o + s = 1$. Furthermore, we define the porous concentration C_o associated with the oil component as the concentration taken with respect to the volume of the pore space occupied by oil and represented by ϕs_o. Hence, C_o and ρ_o are related by

$$\rho_o = \phi s_o C_o. \tag{21}$$

Similarly, the porous concentrations of the various components in the water phase are defined as the concentration taken with respect to the volume of the pores occupied by water ϕs. Consequently, the porous concentrations C_l, C_{na}, C_{cl}, C_{ca}, C_{mg}, and C_{so} are related to the total concentrations by

$$\rho_l = \phi s C_l,\ \rho_{na} = \phi s C_{na},\ \rho_{cl} = \phi s C_{cl},\ \rho_{ca} = \phi s C_{ca},\ \rho_{mg} = \phi s C_{mg},\ \rho_{so} = \phi s C_{so}.$$

Following, for example, [1, 2], we argue that since oil, water, and the ions in water Na^+, Cl^-, Ca^{2+}, Mg^{2+}, and SO_4^{2-} flow only through the pores of the calcite specimen, the "interstitial" velocity $\mathbf{v}_o$ associated with the oil, $\mathbf{v}_l$ associated with the water, and $\mathbf{v}_g$ associated with the ions, have to be defined with respect to the concentrations inside the pores, and differ from the

respective seepage velocities $\mathbf{V}_o$, $\mathbf{V}_l$ and $\mathbf{V}_g$. The velocities are related by the Dupuit-Forchheimer relations, see [1] and references therein,

$$\mathbf{V}_o = \phi s_o \mathbf{v}_o, \qquad \mathbf{V}_l = \phi s \mathbf{v}_l, \qquad \mathbf{V}_g = \phi s \mathbf{v}_g. \tag{22}$$

Consequently, the balance equations (20) can be written in the form

$$\begin{aligned}
\partial_t(\phi s_o C_o) + \nabla \cdot (C_o \mathbf{V}_o) &= 0,\\
\partial_t(\phi s C_l) + \nabla \cdot (C_l \mathbf{V}_l) &= 0,\\
\partial_t(\phi s C_{na}) + \partial_t(M_c \beta_{na}) + \nabla \cdot (C_{na} \mathbf{V}_g) &= 0,\\
\partial_t(\phi s C_{cl}) + \nabla \cdot (C_{cl} \mathbf{V}_g) &= 0,\\
\partial_t(\phi s C_{ca}) + \partial_t(M_c \beta_{ca}) + \nabla \cdot (C_{ca} \mathbf{V}_g) &= 0,\\
\partial_t(\phi s C_{so}) + \nabla \cdot (C_{so} \mathbf{V}_g) &= 0,\\
\partial_t(\phi s C_{mg}) + \partial_t(M_c \beta_{mg}) + \nabla \cdot (C_{mg} \mathbf{V}_g) &= 0.
\end{aligned} \tag{23}$$

In order to close the system we must determine the seepage velocities $\mathbf{V}_o$, $\mathbf{V}_l$ and $\mathbf{V}_g$. For that purpose we consider the concentration of the water phase (brine) C that occupies the pore space as a mixture of water C_l and the various species Na^+, Cl^-, Ca^{2+}, Mg^{2+}, and SO_4^{2-} represented by C_g. In other words,

$$C_g = C_{na} + C_{cl} + C_{ca} + C_{mg} + C_{so}, \qquad C = C_g + C_l. \tag{24}$$

Then, we define the seepage velocity $\mathbf{V}$ associated with C by

$$C\mathbf{V} := C_g \mathbf{V}_g + C_l \mathbf{V}_l. \tag{25}$$

Now we are in a position to rewrite the model in terms of $\mathbf{V}$ and the diffusive velocity $\mathbf{U}_g$ given by

$$\mathbf{U}_g = \mathbf{V}_g - \mathbf{V}. \tag{26}$$

Then the model (23) takes the form

$$\begin{aligned}
\partial_t(\phi s_o C_o) + \nabla \cdot (C_o \mathbf{V}_o) &= 0,\\
\partial_t(\phi s C_l) + \nabla \cdot (C_l \mathbf{V}_l) &= 0,\\
\partial_t(\phi s C_{na}) + \partial_t(M_c \beta_{na}) + \nabla \cdot (C_{na} \mathbf{U}_g) &= -\nabla \cdot (C_{na} \mathbf{V}),\\
\partial_t(\phi s C_{cl}) + \nabla \cdot (C_{cl} \mathbf{U}_g) &= -\nabla \cdot (C_{cl} \mathbf{V}),\\
\partial_t(\phi s C_{ca}) + \partial_t(M_c \beta_{ca}) + \nabla \cdot (C_{ca} \mathbf{U}_g) &= -\nabla \cdot (C_{ca} \mathbf{V}),\\
\partial_t(\phi s C_{so}) + \nabla \cdot (C_{so} \mathbf{U}_g) &= -\nabla \cdot (C_{so} \mathbf{V}),\\
\partial_t(\phi s C_{mg}) + \partial_t(M_c \beta_{mg}) + \nabla \cdot (C_{mg} \mathbf{U}_g) &= -\nabla \cdot (C_{mg} \mathbf{V}).
\end{aligned} \tag{27}$$

Furthermore, we can assume that the seepage velocity $\mathbf{V}$ associated with the water phase represented by C, is given by Darcy's law [1, 7, 26]

$$\mathbf{V} = -\kappa\lambda(\nabla p - \rho g \nabla d), \qquad \lambda = \frac{k}{\mu}, \tag{28}$$

where κ is absolute permeability, k is water relative permeability, and μ is viscosity, and p pressure in water phase. Similarly, for the oil phase

$$\mathbf{V}_o = -\kappa\lambda_o(\nabla p_o - \rho_o g \nabla d), \qquad \lambda_o = \frac{k_o}{\mu_o}. \tag{29}$$

The diffusive velocity $\mathbf{U}_g$ is expressed by Fick's law by

$$C_i \mathbf{U}_g = -D\nabla C_i, \qquad i = na, cl, ca, so, mg, \tag{30}$$

where D is the diffusion coefficient. In view of (24) and (30), it follows that

$$C_g \mathbf{U}_g = -D\nabla C_g. \tag{31}$$

Note that we assume that the diffusion coefficient D is the same for all species $i = na, cl, ca, so, mg$. This is a reasonable assumption as long as the concentration is not too high. D is the diffusion

coefficient (longitudinal and transversal dispersion lengths are here taken to be equal), which is split into molecular diffusion contribution and the so called mechanical/advective contribution. A widely quoted formulation by Sahimi [32] is of the form

$$\frac{D}{D_m} = \phi^p s^q + aP_e + bP_e^\delta + cP_e^2, \tag{32}$$

where D_m is the free molecular diffusion coefficient, $p, q, a, b, c,$ and δ are experimentally determined constants and P_e is the Péclet number given by

$$P_e = \frac{\alpha|\mathbf{V}|}{D_m}, \tag{33}$$

where α is the characteristic dispersion length which varies from millimeters (in laboratory scale) to metres(field scale). Several authors [8, 32] have experimentally determined that the diffusion co-efficient is determined by only the first term of equation(32) when P_e is less than 0.3, and a transition zone between 0.3 and 5 where D is not clearly defined. The other terms of the equation becomes significant at higher Péclet numbers. For our application of the model, the Péclet number falls below 0.3, hence subsequently we use only the first term of equation (32). In (32) the coefficient p is referred to as the cementation exponent, q as the saturation exponent. The cementation exponent is often close to 2 whereas the saturation exponent is also often fixed at a value in the same range, see for example [8, 10, 11]. Using (30) in (27) yields

$$\begin{aligned}
\partial_t(\phi s_o C_o) + \nabla\cdot(C_o\mathbf{V}_o) &= 0,\\
\partial_t(\phi s C_l) + \nabla\cdot(C_l\mathbf{V}_l) &= 0,\\
\partial_t(\phi s C_{na}) + \partial_t(M_c\beta_{na}) - \nabla\cdot(D\nabla C_{na}) &= -\nabla\cdot(C_{na}\mathbf{V}),\\
\partial_t(\phi s C_{cl}) - \nabla\cdot(D\nabla C_{cl}) &= -\nabla\cdot(C_{cl}\mathbf{V}),\\
\partial_t(\phi s C_{ca}) + \partial_t(M_c\beta_{ca}) - \nabla\cdot(D\nabla C_{ca}) &= -\nabla\cdot(C_{ca}\mathbf{V}),\\
\partial_t(\phi s C_{so}) - \nabla\cdot(D\nabla C_{so}) &= -\nabla\cdot(C_{so}\mathbf{V}),\\
\partial_t(\phi s C_{mg}) + \partial_t(M_c\beta_{mg}) - \nabla\cdot(D\nabla C_{mg}) &= -\nabla\cdot(C_{mg}\mathbf{V}).
\end{aligned} \tag{34}$$

In particular, summing the equations corresponding to C_{na}, C_{cl}, C_{ca}, C_{so}, and C_{mg}, we obtain an equation for C_g in the form

$$\partial_t(\phi s C_g) + \partial_t(M_c[\beta_{na} + \beta_{ca} + \beta_{mg}]) - \nabla\cdot(D\nabla C_g) = -\nabla\cdot(C_g\mathbf{V}). \tag{35}$$

In a similar manner, using $C_l\mathbf{V}_l = C_l\mathbf{V} - C_g\mathbf{U}_g$ (obtained from (25), (26), and (24)) in the second equation of (34), the following equation is obtained

$$\partial_t(\phi s C_l) + \nabla\cdot(C_l\mathbf{V}) = \nabla\cdot(C_g\mathbf{U}_g). \tag{36}$$

Summing (36) and (35), we get the following equation for the concentration of the water phase with its different chemical components, represented by $C = C_g + C_l$,

$$\partial_t(\phi s C) + \partial_t(M_c[\beta_{na} + \beta_{ca} + \beta_{mg}]) + \nabla\cdot(C\mathbf{V}) = 0. \tag{37}$$

To sum up, we have a model in the form

$$\begin{aligned}
\partial_t(\phi s_o C_o) + \nabla\cdot(C_o\mathbf{V}_o) &= 0,\\
\partial_t(\phi s C) + \partial_t(M_c[\beta_{na} + \beta_{ca} + \beta_{mg}]) + \nabla\cdot(C\mathbf{V}) &= 0,\\
\partial_t(\phi s C_{na}) + \partial_t(M_c\beta_{na}) + \nabla\cdot(C_{na}\mathbf{V}) &= \nabla\cdot(D\nabla C_{na}),\\
\partial_t(\phi s C_{cl}) + \nabla\cdot(C_{cl}\mathbf{V}) &= \nabla\cdot(D\nabla C_{cl}),\\
\partial_t(\phi s C_{ca}) + \partial_t(M_c\beta_{ca}) + \nabla\cdot(C_{ca}\mathbf{V}) &= \nabla\cdot(D\nabla C_{ca}),\\
\partial_t(\phi s C_{so}) + \nabla\cdot(C_{so}\mathbf{V}) &= \nabla\cdot(D\nabla C_{so}),\\
\partial_t(\phi s C_{mg}) + \partial_t(M_c\beta_{mg}) + \nabla\cdot(C_{mg}\mathbf{V}) &= \nabla\cdot(D\nabla C_{mg}),
\end{aligned} \tag{38}$$

where $D = D(\phi, s)$ as given by (32).

4.1. Simplifying assumptions. Before we proceed some simplifying assumptions are made:

- The oil and water component densities C_o and C are assumed to be constant, i.e., incompressible fluids;
- The effect from the water-rock chemistry in the water phase equation (second equation of (38)) is neglected which is reasonable since the concentration of the water phase C is much larger than the concentrations of the ion exchange involved in the chemical reactions;
- Constant porosity ϕ, absolute permeability κ, viscosities μ, μ_o;
- One dimensional flow in a horizontal domain.
- Capillary pressure is currently neglected as discussed in the introduction (Section 1.2).

This results in the following simplified model:

$$
\begin{aligned}
\partial_t(\phi s_o) + \partial_x(V_o) &= 0,\\
\partial_t(\phi s) + \partial_x(V) &= 0,\\
\partial_t(\phi s C_{na}) + \partial_t(M_c\beta_{na}) + \partial_x(C_{na}V) &= \partial_x(D(\phi,s)\partial_x C_{na}),\\
\partial_t(\phi s C_{cl}) + \partial_x(C_{cl}V) &= \partial_x(D(\phi,s)\partial_x C_{cl}),\\
\partial_t(\phi s C_{ca}) + \partial_t(M_c\beta_{ca}) + \partial_x(C_{ca}V) &= \partial_x(D(\phi,s)\partial_x C_{ca}),\\
\partial_t(\phi s C_{so}) + \partial_x(C_{so}V) &= \partial_x(D(\phi,s)\partial_x C_{so}),\\
\partial_t(\phi s C_{mg}) + \partial_t(M_c\beta_{mg}) + \partial_x(C_{mg}V) &= \partial_x(D(\phi,s)\partial_x C_{mg}).
\end{aligned}
\tag{39}
$$

In view of (28) and (29) in a 1D domain, we get

$$
V = -\kappa\lambda p_x, \qquad \lambda(\beta_{ca},\beta_{mg}) = \frac{k(\beta_{ca},\beta_{mg})}{\mu} \tag{40}
$$

$$
V_o = -\kappa\lambda_o p_{o,x}, \qquad \lambda_o(\beta_{ca},\beta_{mg}) = \frac{k_o(\beta_{ca},\beta_{mg})}{\mu_o}, \tag{41}
$$

Moreover, capillary pressure P_c is defined as the difference between oil and water pressure

$$
P_c = p_o - p, \tag{42}
$$

and is assumed to be zero in the following. Total velocity v_T is given by

$$
v_T := V + V_o = -\kappa(\lambda p_x + \lambda_o p_{o,x}) = -\kappa\lambda_T p_x, \tag{43}
$$

where total mobility λ_T

$$
\lambda_T = \lambda + \lambda_o, \tag{44}
$$

has been introduced. Summing the two first equations of (39) and using that $1 = s+s_o$, implies that $(v_T)_x = 0$, i.e., v_T =constant and is determined, for example, from the boundary conditions. From the continuity equation for s given by the second equation of (39) it follows (since $V = -\kappa\lambda p_x$)

$$
(\phi s)_t + (-\kappa\lambda p_x)_x = 0, \tag{45}
$$

where, in view of (43),

$$
-\kappa p_x = \frac{v_T}{\lambda_T}.
$$

Thus,

$$
(\phi s)_t + (v_T\frac{\lambda}{\lambda_T})_x = 0. \tag{46}
$$

The fractional flow functions $f(\beta_{ca},\beta_{mg})$ and $f_o(\beta_{ca},\beta_{mg})$ are defined as follows

$$
f(s,\beta_{ca},\beta_{mg}) \stackrel{\text{def}}{:=} \frac{\lambda(s,\beta_{ca},\beta_{mg})}{\lambda(s,\beta_{ca},\beta_{mg}) + \lambda_o(\beta_{ca},\beta_{mg})}, \tag{47}
$$

$$
f_o(s,\beta_{ca},\beta_{mg}) \stackrel{\text{def}}{:=} \frac{\lambda_o(s,\beta_{ca},\beta_{mg})}{\lambda(s,\beta_{ca},\beta_{mg}) + \lambda_o(\beta_{ca},\beta_{mg})} = 1 - f(\beta_{ca},\beta_{mg}). \tag{48}
$$

Using this in (46) implies that

$$
(\phi s)_t + v_T f(s,\beta_{ca},\beta_{mg})_x = 0. \tag{49}
$$

The same procedure can be applied for the continuity equation for the different ions in water in (39). This gives the following equation for $i = na, cl, ca, so, mg$:

$$(\phi s C_i)_t + (M_c \beta_i)_t + v_T (C_i f(s, \beta_{ca}, \beta_{mg})_x = (D(\phi, s) C_{i,x})_x, \qquad i = na, cl, ca, so, mg. \tag{50}$$

Thus, in view of (49) and (50), a model has been obtained of the form

$$\begin{aligned}
\partial_t(\phi s) + v_T \partial_x f(s, \beta_{ca}, \beta_{mg}) &= 0, \\
\partial_t(\phi s C_{na} + M_c \beta_{na}) + v_T \partial_x (C_{na} f(s, \beta_{ca}, \beta_{mg})) &= \partial_x (D(\phi, s) \partial_x C_{na}), \\
\partial_t(\phi s C_{cl}) + v_T \partial_x (C_{cl} f(s, \beta_{ca}, \beta_{mg})) &= \partial_x (D(\phi, s) \partial_x C_{cl}), \\
\partial_t(\phi s C_{ca} + M_c \beta_{ca}) + v_T \partial_x (C_{ca} f(s, \beta_{ca}, \beta_{mg})) &= \partial_x (D(\phi, s) \partial_x C_{ca}) \\
\partial_t(\phi s C_{so}) + v_T \partial_x (C_{so} f(s, \beta_{ca}, \beta_{mg})) &= \partial_x (D(\phi, s) \partial_x C_{so}), \\
\partial_t(\phi s C_{mg} + M_c \beta_{mg}) + v_T \partial_x (C_{mg} f(s, \beta_{ca}, \beta_{mg})) &= \partial_x (D(\phi, s) \partial_x C_{mg}).
\end{aligned} \tag{51}$$

4.2. Scaled version of the model. First, we introduce the variables

$$c_1 := \phi s C_{na}, \quad c_2 := \phi s C_{cl}, \quad c_3 := \phi s C_{ca}, \quad c_4 := \phi s C_{so}, \quad c_5 := \phi s C_{mg}. \tag{52}$$

We also introduce the variables

$$B_1 = M_c \beta_{na}(C_{na}, C_{ca}, C_{mg}), \quad B_3 = M_c \beta_{ca}(C_{na}, C_{ca}, C_{mg}), \quad B_5 = M_c \beta_{mg}(C_{na}, C_{ca}, C_{mg}). \tag{53}$$

Now let L be the the reference length, which here is chosen to be the length of the core. As time scale of the problem τ (sec) we use

$$\tau = \frac{\phi L}{v_T}. \tag{54}$$

We then define dimensionless space x' and time t' variables as follows

$$x' = \frac{x}{L}, \qquad t' = \frac{t}{\tau}. \tag{55}$$

We introduce reference viscosity $\overline{\mu}$ (Pa s), and reference diffusion coefficient $\overline{D}_m$ (m^2/s). Then we define dimensionless coefficients

$$D'_m = \frac{D_m}{\overline{D}_m}, \qquad \mu' = \frac{\mu}{\overline{\mu}}. \tag{56}$$

Rewriting (51) in terms of the dimensionless space and time variables (55) and using (56), the following form of the system is obtained (skipping the prime notation)

$$\partial_t(\phi s) + \partial_x(\phi f(s, \beta_{ca}, \beta_{mg})) = 0, \tag{57}$$

$$\begin{aligned}
\partial_t(c_1 + B_1(c_1, c_3, c_5)) + \partial_x(C_{na} \phi f(s, \beta_{ca}, \beta_{mg})) &= \delta \partial_x(D_m \phi^p s^q \partial_x C_{na}), \\
\partial_t(c_2) + \partial_x(C_{cl} \phi f(s, \beta_{ca}, \beta_{mg})) &= \delta \partial_x(D_m \phi^p s^q \partial_x C_{cl}), \\
\partial_t(c_3 + B_2(c_1, c_3, c_5)) + \partial_x(C_{ca} \phi f(s, \beta_{ca}, \beta_{mg})) &= \delta \partial_x(D_m \phi^p s^q \partial_x C_{ca}), \\
\partial_t(c_4) + \partial_x(C_{so} \phi f(s, \beta_{ca}, \beta_{mg})) &= \delta \partial_x(D_m \phi^p s^q \partial_x C_{so}), \\
\partial_t(c_5 + B_3(c_1, c_3, c_5)) + \partial_x(C_{mg} \phi f(s, \beta_{ca}, \beta_{mg})) &= \delta \partial_x(D_m \phi^p s^q \partial_x C_{mg}),
\end{aligned} \tag{58}$$

where the dimensionless characteristic number δ, is given by

$$\delta = \frac{\phi \overline{D}_m}{L v_T}. \tag{59}$$

We choose $\overline{D}_m = L v_T$ in (56) such that $\delta = \phi$.

4.3. Boundary and initial conditions. In order to have a well defined system to solve we must specify appropriate initial and boundary conditions.

4.3.1. Boundary conditions. At the inlet, the following Dirichlet boundary conditions are employed

$$s(0^-,t) = s(1^+,t) = 1.0, \qquad C_i(0^-,t) = C_i(1^+,t) = C_i^*, \tag{60}$$

for the species $i = na, cl, ca, so, mg$ where C_i^* is the specified ion concentrations of the brine that is used. At the outlet extrapolation is employed both for s and the C_i's.

4.3.2. Initial data. Initially, the plug is filled with oil and 15.0% formation water. Thus, initial data are given by

$$s|_{t=0}(x) = s_{\text{init}} = 0.15, \qquad x \in [0,1], \tag{61}$$

and for $i = na, cl, ca, so, mg$,

$$C_i|_{t=0}(x) = C_{i,0}, \qquad x \in [0,1], \tag{62}$$

for given initial concentration of the species $C_{i,0}$ in the water phase (formation water).

5. Numerical discretization

The numerical discretization of the resulting nonlinear convection-diffusion system is based on the same approach as that used in [45, 46], and we refer to these works for more details. However, for completeness we briefly sketch the discretization of the nonlinear convective term. The diffusion term is discretized by using a standard central discretization.

5.1. Discretization of convective flux. Consider now a system of conservation laws in one space variable

$$\partial_t \mathbf{w} + \partial_x F(\mathbf{w}) = 0, \tag{63}$$

where $F(\mathbf{w}) \in \mathbb{R}^n$ is a smooth vector-valued function. The discretization of the nonlinear convective (advective) flux is based on the relaxed scheme by Jin and Xin [23]. The relaxed scheme can be written in the following "viscous" form

$$\begin{cases} \mathbf{w}_j^{n+1} = \mathbf{w}_j^n - \lambda(\hat{F}_{j+1/2}^n - \hat{F}_{j-1/2}^n), \qquad \lambda = \frac{\Delta t}{\Delta x} \\ \text{where} \\ \hat{F}_{j+1/2} = \frac{1}{2}\Big(F(\mathbf{w}_j) + F(\mathbf{w}_{j+1})\Big) - \frac{1}{2}A^{1/2}(\mathbf{w}_{j+1} - \mathbf{w}_j), \end{cases} \tag{64}$$

where $A^{1/2}$ plays the role as the "viscosity matrix" which determines the numerical dissipation of the scheme. Here we must require that the well known subcharacteristic condition holds given by

$$A - F'(\mathbf{w})^2 \geq 0, \qquad \text{for all } \mathbf{w}. \tag{65}$$

In our case it suffices to choose that A has the special form

$$A = aI, \qquad a > 0 \tag{66}$$

where I is the identity matrix. In the case of one space variable (as we consider) and where we assume (66), the dissipative condition (65) is satisfied if

$$\lambda^2 < a, \tag{67}$$

where $\lambda = \max_{1\leq i\leq n} |\lambda_i(\mathbf{w})|$ where λ_i are the genuine eigenvalues of $F'(\mathbf{w})$.

The relaxed scheme (64) can also be viewed as a flux splitting scheme. To see this we write the system as

$$\begin{cases} \mathbf{w}_j^{n+1} = \mathbf{w}_j^n - \lambda(\hat{F}_{j+1/2}^n - \hat{F}_{j-1/2}^n) \\ \text{where} \\ \hat{F}_{j+1/2} = F_{j+1/2,-}^+ + F_{j+1/2,+}^-, \end{cases} \tag{68}$$

where we have (for the first order scheme) that

$$F_{j+1/2,-}^+ = F^+(\mathbf{w}_j), \qquad F_{j+1/2,+}^- = F^-(\mathbf{w}_{j+1}),$$

and where we have used the Lax-Friedrichs flux splitting

$$F^{\pm}(\mathbf{w}) = \frac{1}{2}(F(\mathbf{w}) \pm A^{1/2}\mathbf{w}). \tag{69}$$

Note that the condition (65) ensures that the Jacobian of $F^{\pm}(\mathbf{w})$ has nonnegative eigenvalues only or nonpositive eigenvalues only.

The second order relaxed scheme can be obtained by using van Leer's MUSCL scheme. Instead of using the piecewise constant interpolation, MUSCL uses the piecewise linear interpolation which, when it is applied to the p-th components of $F^{+}(\mathbf{w}_j)$ approximated at x_j, yields:

$$\begin{aligned} &(F^{+})_j^{(p)}(x) = (F^{+})^{(p)}(\mathbf{w}_j) + (S^{+})_j^{(p)}(x - x_j), \qquad x \in (x_{j-1/2}, x_{j+1/2}) \\ &\text{where} \\ &(S^{+})_j^{(p)} = S((s_l^{+})^{(p)}, (s_r^{+})^{(p)}) \end{aligned} \tag{70}$$

and

$$(s_l^{+})^p = \frac{(F^{+})^{(p)}(\mathbf{w}_j) - (F^{+})^{(p)}(\mathbf{w}_{j-1})}{\Delta x}, \qquad (s_r^{+})^p = \frac{(F^{+})^{(p)}(\mathbf{w}_{j+1}) - (F^{+})^{(p)}(\mathbf{w}_j)}{\Delta x}.$$

Here $S(u, v)$ represents the slope limiter function. Similarly, the piecewise linear interpolation applied to the p-th components of the negative flux part $F^{-}(\mathbf{w}_{j+1})$ approximated at x_{j+1} yields:

$$\begin{aligned} &(F^{-})_{j+1}^{(p)}(x) = (F^{-})^{(p)}(\mathbf{w}_{j+1}) + (S^{-})_{j+1}^{(p)}(x - x_{j+1}), \qquad x \in (x_{j+1/2}, x_{j+3/2}) \\ &\text{where} \\ &(S^{-})_{j+1}^{(p)} = S((s_l^{-})^{(p)}, (s_r^{-})^{(p)}) \end{aligned} \tag{71}$$

and

$$(s_l^{-})^p = \frac{(F^{-})^{(p)}(\mathbf{w}_{j+1}) - (F^{-})^{(p)}(\mathbf{w}_j)}{\Delta x}, \qquad (s_r^{-})^p = \frac{(F^{-})^{(p)}(\mathbf{w}_{j+2}) - (F^{-})^{(p)}(\mathbf{w}_{j+1})}{\Delta x}.$$

The van Leer limiter corresponds to the choice

$$S(u, v) = s(u, v)\frac{2|u||v|}{|u| + |v|}, \tag{72}$$

where $s(u, v) = 1/2(\mathrm{sgn}(u) + \mathrm{sgn}(v))$. The numerical flux $F_{j+1/2}^{(p)}$ is then computed in a split form,

$$\hat{F}_{j+1/2}^{(p)} = (F^{+})_j^{(p)}(x)|_{x_{j+1/2}} + (F^{-})_{j+1}^{(p)}(x)|_{x_{j+1/2}}. \tag{73}$$

Second order accuracy in time can be obtained by using a two-stage Runge-Kutta discretization. We chose to employ a standard forward Euler since this required less time and main purpose of simulations was to evaluate impact from the ion exchange process on the two-phase flow behavior.

5.2. Generally. A main difference between the current model and the one discussed in [45] is that a more complicated nonlinear system of algebraic equations must be solved due to the multiple ion exchange process. In contrast, [45, 46] considered only a single adsorption isotherm. In order to describe this more precisely, let us introduce the vector

$$\mathbf{E} = (c_1 + B_1(c_1, c_3, c_5, \phi s), c_2, c_3 + B_3(c_1, c_3, c_5, \phi s), c_4, c_5 + B_5(c_1, c_3, c_5, \phi s))^T, \tag{74}$$

and

$$\mathbf{C} = (c_1, c_2, c_3, c_4, c_5)^T. \tag{75}$$

We assume that we have approximate solutions $(s^n, \mathbf{C}^n)(\cdot) \approx (s, \mathbf{C})(\cdot, t^n)$. Now, we want to calculate an approximation at the next time level $(s^{n+1}, \mathbf{C}^{n+1})(\cdot) \approx (s, \mathbf{C})(\cdot, t^{n+1})$. The system of parabolic PDEs given by equations (57) and (58), which we solve for $t \in (0, \Delta t]$, is in the form

$$\begin{aligned} \partial_t s + \partial_x f(s, \mathbf{C}) &= 0, & s(\cdot, 0) &= s^n(\cdot), \\ \partial_t \mathbf{E} + \partial_x \mathbf{F}(s, \mathbf{C}) &= \partial_x(\mathbf{D}(s)\partial_x(\mathbf{C}/s)), & \mathbf{C}(\cdot, 0) &= \mathbf{C}^n(\cdot), \end{aligned} \tag{76}$$

for suitable choices of $\mathbf{F}$ and $\mathbf{D}$. Then we find $(s^{n+1}, \mathbf{E}^{n+1})$. Finally, in order to proceed to the next time step, we must compute $\mathbf{C}^{n+1} = \mathbf{H}(\mathbf{E}^{n+1})$, where the latter equation is a nonlinear algebraic equation, which can be written as

$$(c_1+B_1(c_1,c_3,c_5,\phi s^{n+1}), c_2, c_3+B_3(c_1,c_3,c_5,\phi s^{n+1}), c_4, c_5+B_5(c_1,c_3,c_5,\phi s^{n+1}))^T = \mathbf{E}^{n+1}. \tag{77}$$

Note that the above equations are nonlinear in the variables c_1, c_3 and c_5, but is a straightforward identity for c_2 and c_4. By solving equation (77) numerically, we obtain $\mathbf{C}^{n+1}$. We describe the procedure in the next subsection. However, we should also note that the chemical activity coefficients $\gamma_i = \gamma_i(I_0)$ for species i, are updated before every new time step in our numerical procedure by using the concentrations $C_{na}, C_{cl}, C_{ca}, C_{so}, C_{mg}$ obtained from $\mathbf{C}$, in equations (4) and (5), as explained in Section 2.1.

5.3. Solving the nonlinear system. It is seen by looking at the equations (11), (12) and (13), and using the definition (53) that

$$B_1 = \widetilde{C}_1 \frac{c_1}{\sqrt{c_3}} B_3, \tag{78}$$

and

$$B_5 = \widetilde{C}_3 \frac{\sqrt{c_5}}{\sqrt{c_3}} B_3, \tag{79}$$

where

$$\widetilde{C}_1 = \frac{\gamma_{na}}{\sqrt{\phi s^{n+1}\gamma_{ca}} K_{cana}}, \tag{80}$$

and

$$\widetilde{C}_3 = \frac{\sqrt{\gamma_{mg}} K_{mgna}}{\sqrt{\gamma_{ca}} K_{cana}}. \tag{81}$$

Now using (78) as well as the first and third equations in (77), it is easily found that

$$c_1 = \frac{\sqrt{x} E_1^{n+1}}{\sqrt{x} + \widetilde{C}_1 (E_3^{n+1} - x)}, \tag{82}$$

where we have set $x := c_3$. Likewise, (79) can be used in combination with the third and fifth equations in (77) to establish the equation

$$c_5 \sqrt{x} + \widetilde{C}_3 (E_3^{n+1} - x)\sqrt{c_5} = E_5^{n+1}\sqrt{x}. \tag{83}$$

We note from (83) that if x is equal to zero then $c_5 = 0$. If $x > 0$ then let

$$\widetilde{B} = \frac{\widetilde{C}_3 (E_3^{n+1} - x)}{\sqrt{x}}, \tag{84}$$

and

$$w = \sqrt{c_5}, \qquad (c_5 = w^2), \tag{85}$$

in order to obtain the second order equation

$$w^2 + \widetilde{B} w - E_5^{n+1} = 0, \tag{86}$$

which has the physical solution

$$w = w(x) = \frac{-\widetilde{B}(x) + \sqrt{\widetilde{B}(x)^2 + 4E_5^{n+1}}}{2}. \tag{87}$$

Finally, using the third equation in (77) i.e.

$$x + B_3(c_1(x), x, c_5(x), \phi s^{n+1}) = E_3^{n+1}, \tag{88}$$

and substituting the expressions for $c_1(x)$ and $c_5(x)$, found from the equations (82), (85), and (87) above, in B_3, we arrive at the following nonlinear equation in the variable x (in light of (12) and (52)):

$$x + \frac{g(x)}{h(x)} - E_3^{n+1} = 0, \tag{89}$$

where

$$g(x) = M_c CEC \sqrt{\gamma_{ca}} K_{cana} \sqrt{x}, \tag{90}$$

and

$$\begin{aligned} h(x) &= 2K_{cana}\sqrt{\gamma_{ca}}\sqrt{x} + \frac{\gamma_{na}}{\sqrt{\phi s^{n+1}}}\Big(\frac{\sqrt{x}E_1^{n+1}}{\sqrt{x} + \widetilde{C}_1(E_3^{n+1} - x)}\Big) \\ &+ K_{mgna}\sqrt{\gamma_{mg}}\Big(- \frac{\widetilde{C}_3(E_3^{n+1} - x)}{\sqrt{x}} + \sqrt{\frac{(\widetilde{C}_3(E_3^{n+1} - x))^2}{x} + 4E_5^{n+1}} \ \Big). \end{aligned} \tag{91}$$

Currently, we solve the nonlinear equation (89) by using the matlab routine *fzero*.

5.4. Numerical treatment of the selectivity factors. A number of authors have shown that the selectivity factors may vary with brine salinity and concentrations in a complex way. See [4, 20] for examples of such relations. For the MIE model represented by (6) we see that the selectivity factors we have to deal with are K_{cana} and K_{mgna}. For ease of computations we interpolate linearly between two extreme values of selectivity factors K_{mgna}^{LS} and K_{mgna}^{HS}, corresponding to low salinity brine concentrations B_s^{LS} and high salinity brine concentrations B_s^{HS} respectively:

$$\begin{aligned} K_{mgna}(B_s) &= \Big(\frac{B_s^{HS} - B_s}{B_s^{HS} - B_s^{LS}}\Big)K_{mgna}^{LS} + \Big(\frac{B_s - B_s^{LS}}{B_s^{HS} - B_s^{LS}}\Big)K_{mgna}^{HS} \\ K_{cana}(B_s) &= \Big(\frac{B_s^{HS} - B_s}{B_s^{HS} - B_s^{LS}}\Big)K_{cana}^{LS} + \Big(\frac{B_s - B_s^{LS}}{B_s^{HS} - B_s^{LS}}\Big)K_{cana}^{HS}, \end{aligned} \tag{92}$$

where Brine salinity B_s is given by

$$B_s = \sum_i C_i Z_i. \tag{93}$$

Note that the selectivity factors are updated at each grid block for every new time step by using values of the brine salinity from the previous time step. We refer to Appendix A for specific choices of B_s^{LS} and B_s^{HS} as well as $K_{mgna}^{LS}, K_{mgna}^{HS}$ and $K_{cana}^{LS}, K_{cana}^{HS}$.

6. Numerical investigations

6.1. Generally. The core plug under consideration is initially filled with formation water which is in equilibrium with the ions on the rock surface. Initially, the core plug has a given wetting state, termed here as *high salinity* wetting state, which is completely described by its relative permeability functions, see Section 3.1. However, when flooding is done with a brine with ion concentrations different from the formation water, the invading brine creates concentration fronts that move with a certain speed. At these fronts, as well as behind them, chemical interactions in terms of a multiple ion exchange process will take place. It is expected that the water-rock interaction then can lead to a change of the wetting state such that more oil can be mobilized. Main focus of this paper has been, motivated by previous experimental research as described in Section 1, to build into the model a mechanism that relates wettability alteration (towards a *low salinity* wetting state) to desorption of divalent cations from the rock surface. The purpose of this computational section is to gain some general insight into the behavior of this model, when performing water flooding with different brines. Obviously, we are particularly interested to see whether we can discover any "low salinity effects" on the oil recovery curves produced by the numerical model.

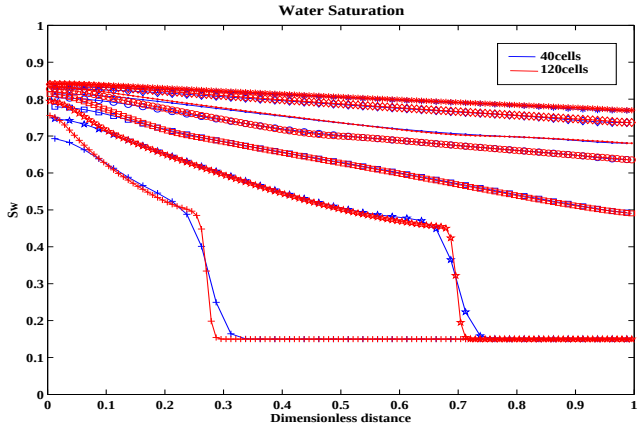

FIGURE 3. Saturation profiles computed with 40 and 120 grid cells, respectively. The comparison is taken from SW flooding (Example 1, case 2).

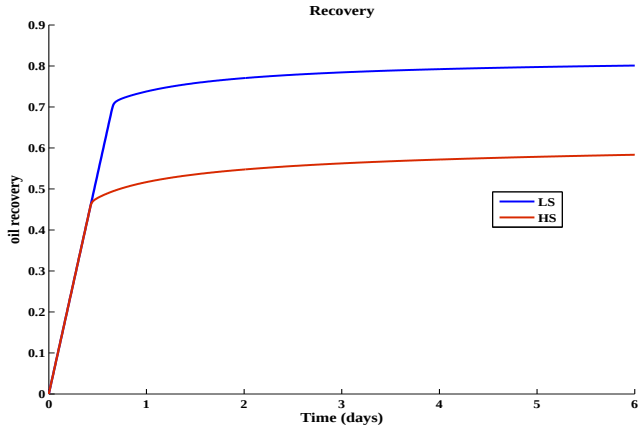

FIGURE 4. Plot showing the recoveries for HS and LS relative permeability curves given in Fig. 2.

6.2. Various data needed for the water flooding simulations. A range of input parameters must be specified for the above model, and are given in Appendix A and B. We emphasize that we will use a *fixed* set of parameters for all simulations, unless anything else is clearly stated. The only change from one simulation to another is the brine composition and/or formation water composition (initial condition).

6.3. A remark on the numerical resolution in the simulations. As stated earlier, the equation systems are solved explicitly. We think that the solutions provided by the explicit method in this paper are sufficient for our present purpose, since we are interested in investigating the fundamental behavior of our one dimensional model. We first present a simulation case where we demonstrate convergence of the numerical solution. We have considered formation water FW and flooding water SW with ion concentrations as described in Table 2 in Appendix A. We have computed solutions on a grid of 40 cells and 120 cells, respectively. Result for the water saturation at different times is shown in Fig. 3. We conclude that it is sufficient to compute solutions on a grid of 40 cells. This will be done in the remaining part of the work.

Before we start exploring how oil recovery can be sensitive for the brine composition of the water that is used for flooding, we show two extremes: Oil recovery for the high salinity conditions

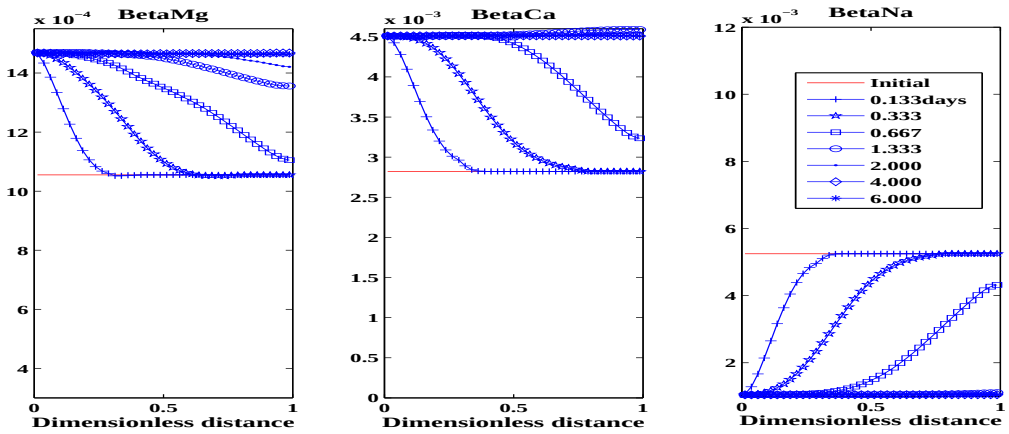

FIGURE 5. Plots showing the behavior of the various β-functions along the core at different times during a time period of 6 days, for the case with LSW as the invading low salinity brine. Note that there is no desorption of the divalent ions (calcium and magnesium), only adsorption. **Left**: β_{mg}. **Middle**: β_{ca}. **Right**: β_{na}.

represented by relative permeability curves (15) versus oil recovery for the low salinity conditions represented by relative permeability curves (16). See also Appendix B for specific data used for the relative permeability functions. Results are shown in Fig. 4. This information is useful to have in mind when we in the remaining part of this section consider brine-dependent oil recovery curves.

6.4. Example 1: Water flooding using different brines and fixed formation water. Here we present simulations of corefloods. The core is composed of clay and other minerals that are assumed to be relatively chemically nonreactive typical of sandstone cores. The clay content/mass of the core is given by M_c(Kg/Liter of core) and clay capacity by CEC (moles/kg of clay), see Appendix A for values. Initially the core is at equilibrium with formation water at initial water saturation, $S_{wi} = 0.15$, and oil. Subsequently, we flood the core with an invading brine at a flow velocity $v_T = 0.01$ (meters/day) for a sufficiently long time, t days, till no appreciable oil is obtained from the core. The runs made in Example 1 are grouped into two groups: *Case 1* in which we inject with a low salinity water and other brines modified from low salinity water (see Table 1 in Appendix A) and *Case 2* in which we inject seawater and other seawater based brines (see Table 2 in Appendix A).

6.4.1. Case 1: Injecting low salinity water and low salinity modified brines. For the different runs in this section, we inject with low salinity brine, LSW and modified low salinity brines LSW1, LSW2 and LSW3. LSW is obtained by a 100 times dilution of formation water. LSW1 by 10 times dilution of formation water. LSW2 by reducing the magnesium component in LSW1 and LSW3 by reducing both divalent ions in LSW1. The brine compositions are given in Table 1 and all other parameters used in the runs are listed in appendix A and B.

Fig. 5 shows the β-functions, which describe the amount of Mg^{2+}, Ca^{2+}, and Na^{+}-ions bonded to the core, for injection of LSW brine. Initially, the formation brine is at equilibrium with the rock, hence, there is a fixed amount of each ion bonded to the surface of the rock. This is denoted by the red curve in Fig. 5. On flooding the core with LSW, this equilibrium is disturbed and a new one is reached after some time. From the figure it is seen that there is no *desorption* of any of the divalent ions (calcium and magnesium) but rather *adsorption* of the divalent ions and desorption of the monovalent ion (sodium). Consequently, the H-function, which is the weighting factor for flow function alteration, remains equal to 1 at all times as shown in Fig. 7. We also show in Fig 6 various ion concentrations C_{ca}, C_{mg}, C_{na}, and C_{cl}.

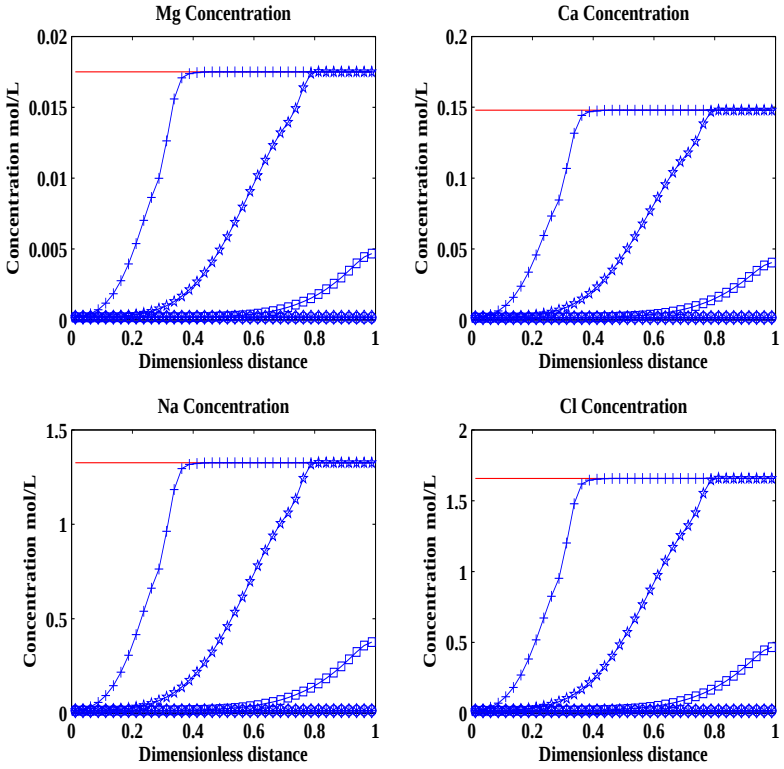

FIGURE 6. Concentrations for different ions for the case with LSW as the invading low salinity brine. **Top Left**: Mg^{2+} concentration. **Top Right**: Ca^{2+} concentration. **Bottom Left**: Na^{2+} concentration. **Bottom Right**: Cl^{-} concentration.

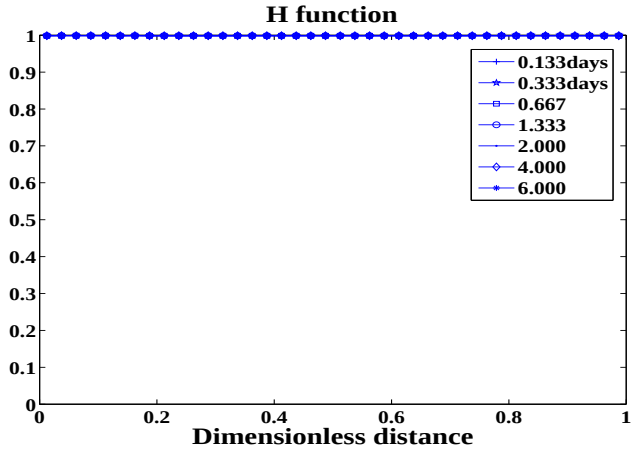

FIGURE 7. The H-function, see equation 18, corresponding to the β-functions for LSW injection.There is no change in H because there is no desorption of divalent ions in Fig. 5.

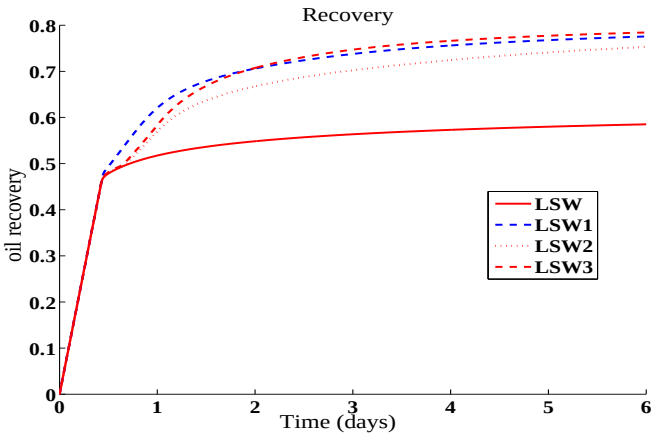

FIGURE 8. Oil recovery for different invading low salinity brines. LSW showing the least recovery since there was no change in H-function in Fig. 7.

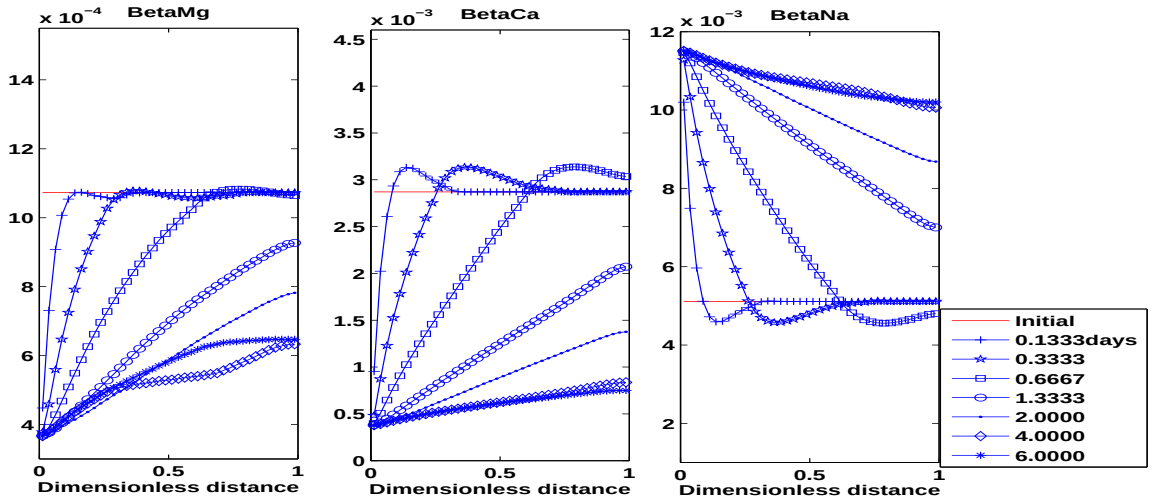

FIGURE 9. Plots showing the various β-functions along the core at different times during a time period of 6 days, for the case with LSW3 as the invading low salinity brine. Note that there is desorption of both divalent ions. **Left**: β_{mg}. **Middle**: β_{ca}. **Right**: β_{na}.

Clearly, when LSW brine is injected there is no positive low salinity effect in terms of improved oil recovery, see Fig. 8. However, the injection of the modified low salinity brines, LSW1, LSW2, and LSW3 led to different degrees of desorption of the divalent ions. Fig. 9 shows desorption of magnesium and calcium ions during LSW3 flooding. Fig. 10 shows the corresponding change in the H-function which moves from 1 towards a lower value as a result of the desorption of calcium and magnesium ions originally attached to the rock. This leads to an almost immediate improved flow of oil behind the water front. See Fig. 11 for a comparison of the water front behavior for LSW3 versus LSW.

The main difference between the low salinity brines LSW1, LSW2, and LSW3, is that LSW2 leads to a desorption of calcium ions only, LSW1 leads to a greater desorption of calcium ions, whereas LSW3 leads to desorption of both magnesium and calcium ions. This is the explanation for the various recoveries seen in Fig. 8.

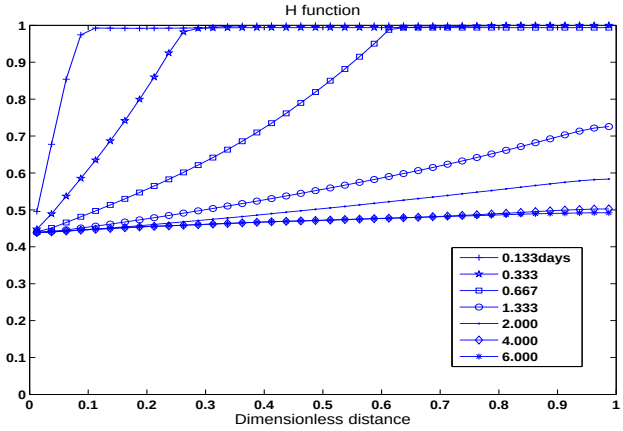

FIGURE 10. The H-function for LSW3 injection corresponding to the β-functions given in Fig. 9. The change from 1 is as a result of desorption of both divalent ions Ca^{2+} and Mg^{2+} during LSW3 injection.

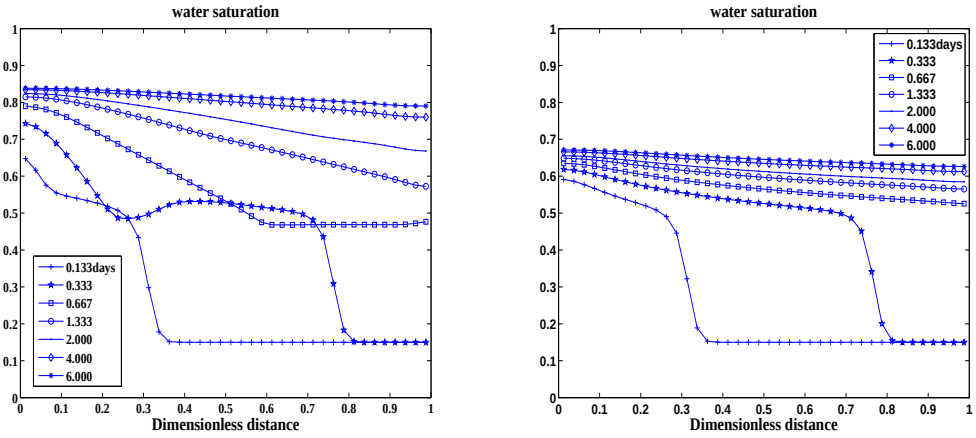

FIGURE 11. Plots showing the water saturation s along the core, for different invading low salinity brines, at different times during a time period of 6 days. The remobilization of oil behind the water front is seen in LSW3. **Left**: LSW3. **Right**: LSW.

6.4.2. Case 2: Injecting seawater and seawater modified brines. Similar runs as in Example 1, case 1, were made but this time injecting with the sea water brine SW and modified sea water brines SW1 and SW2, see Table 2. SW1 is obtained by a 10 times dilution of sea water and SW2 by reducing the calcium component in SW1. The brine compositions are given in table 3.

Flooding with seawater, SW, and the seawater modified brines, SW1 and SW2, the model predicts different degrees of desorption of calcium and adsorption of magnesium ions. Figs. 12 and 13 show the desorption/adsorption on the rock surface for SW and SW2 injection, respectively. It can be seen from the plots that the desorption of calcium is stronger for SW2 injection. This stronger calcium stripping is responsible for the stronger response to favorable wettability alteration typified by a lower H-function in SW2 injection (Fig. 15) than in SW injection (Fig. 14), and consequently a better recovery of SW2 (Fig. 17). SW1 gives the lowest desorption of calcium ions, hence it also gives the lowest recovery. Note that according to equations (17) and (18), only

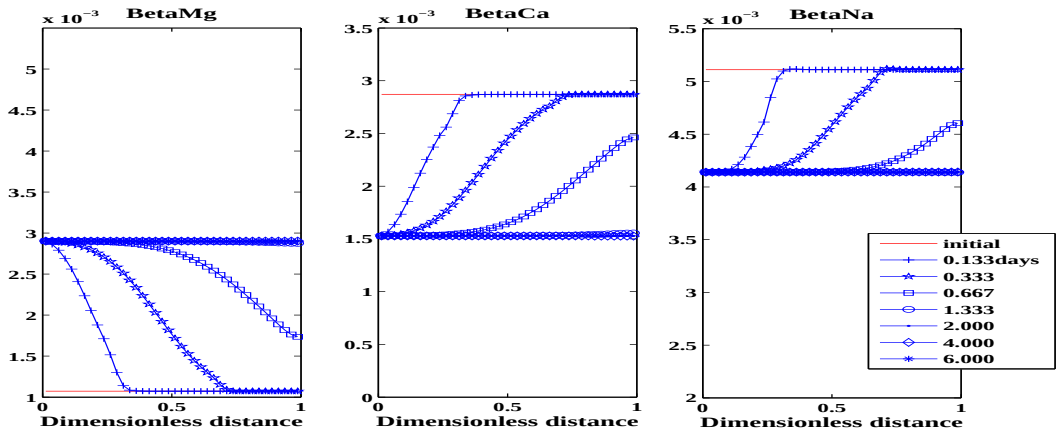

FIGURE 12. Plots showing the behavior of the various β-functions along the core at different times during a time period of 6 days, for the case with SW as the invading sea water brine. Calcium ion is the only desorbed divalent ion. **Left**: β_{mg}. **Middle**: β_{ca}. **Right**: β_{na}.

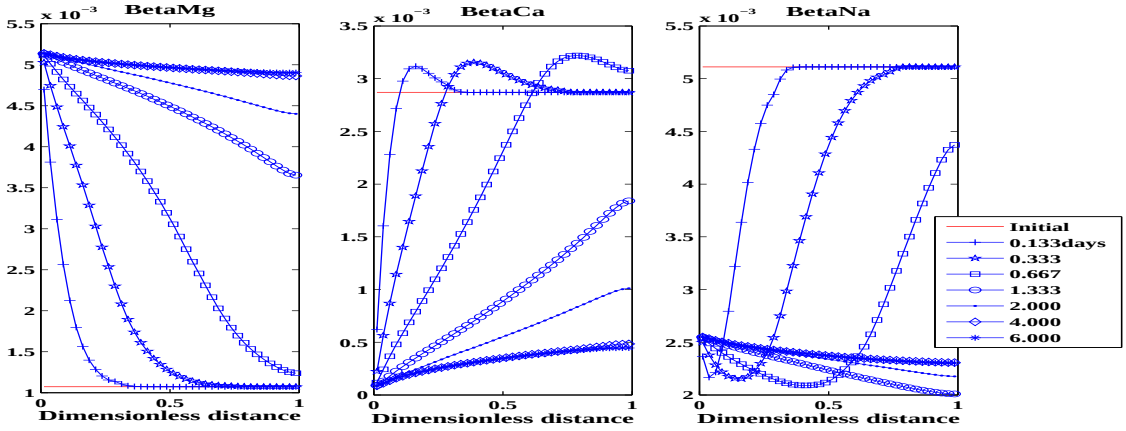

FIGURE 13. Plots showing the behavior of the various β-functions along the core at different times during a time period of 6 days, for the case with SW2 as the invading sea water brine.A stronger calcium desorption is seen here than in Fig. 12. **Left**: β_{mg}. **Middle**: β_{ca}. **Right**: β_{na}.

calcium desorption contributed to the change in the H-function since there was no desorption of magnesium ions in these floods.

Another significant difference in the SW and SW2 injection is the rate of the calcium stripping and subsequently the rate of the wettability alteration. It can be seen in Figs. 12 and 13 that the calcium stripping is faster with SW injection than in SW2 injection. The effect of the above is clearly seen in Fig. 17 where SW recovery is better than SW2 recovery in the early stages and in Fig. 16, where there is no immediate improved oil flow behind the water front in SW2 injection.

6.5. Example 2: Water flooding using different formation waters and a fixed invading brine. For the runs made in this section, we vary the initial formation water FW, FW1 and FW2 and flood with a fixed low salinity water LSW in order to demonstrate the effect that the initial formation water may have in low salinity recovery. FW and LSW are the formation water and low salinity brines used in Example 1. FW1 is derived from FW by increasing the magnesium and

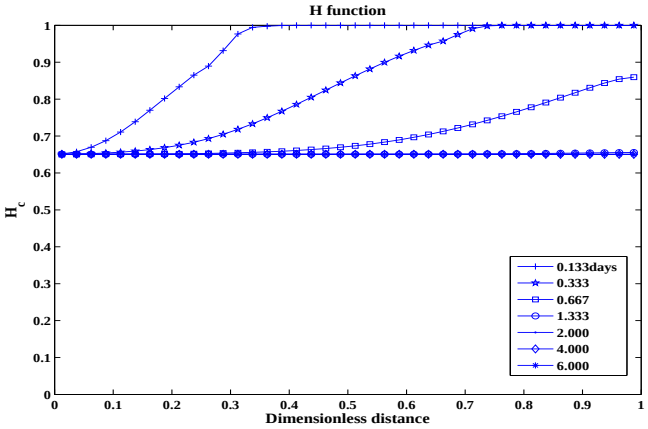

FIGURE 14. The H-function for SW injection corresponding to the β-functions given in Fig. 12.

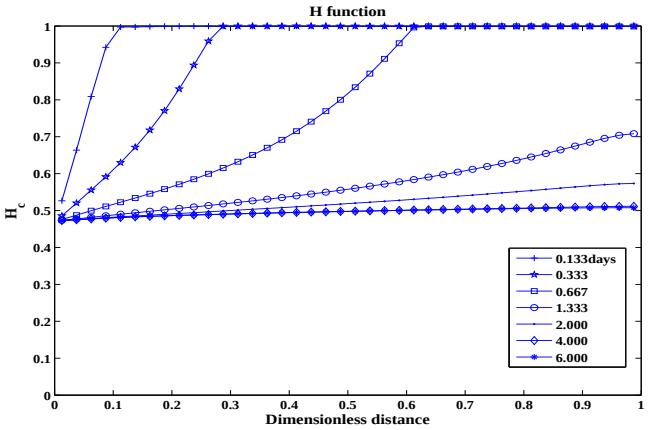

FIGURE 15. The H-function for SW2 corresponding to the β-functions given in Fig. 13. The improved H-function is as a result of the stronger calcium desorption in Fig. 13.

chloride concentration. FW2 is a seawater-like brine. Full description of the brines that are used are given in Table 3. The results show that the initial formation water can play an important role in the recovery that it is obtained. Using FW1 as the formation water clearly gives a higher recovery than FW and FW2 when low salinity water LSW is injected (Fig. 18). This is because the initial state of the core with FW1 brine, promotes more divalent ions on the core surface than either with FW or FW2. Hence subsequent flooding with LSW brine desorbs more of these divalent ions when FW1 is used as the initial brine.

6.6. Example 3: Water flooding showing the effect of clay content and capacity on the concentration profiles. Here we present an example to illustrate the effect of the clay content M_c and cation exchange capacity of the clay, CEC, on the concentration profiles generated along the core. To demonstrate this effect, a CEC of 1.3 eq/Kg of clay and M_c of 0.088 Kg/Litre of core were used. The initial formation water and invading brines are FW and IB, respectively. Their compositions are given in Table 4. It can be seen in Fig. 19 that there is adsorption of calcium and magnesium ions and desorption of sodium ions. The increased adsorption and desorption seen in Fig. 19 is as a result of the high CEC and M_c values used in this example. Note that a

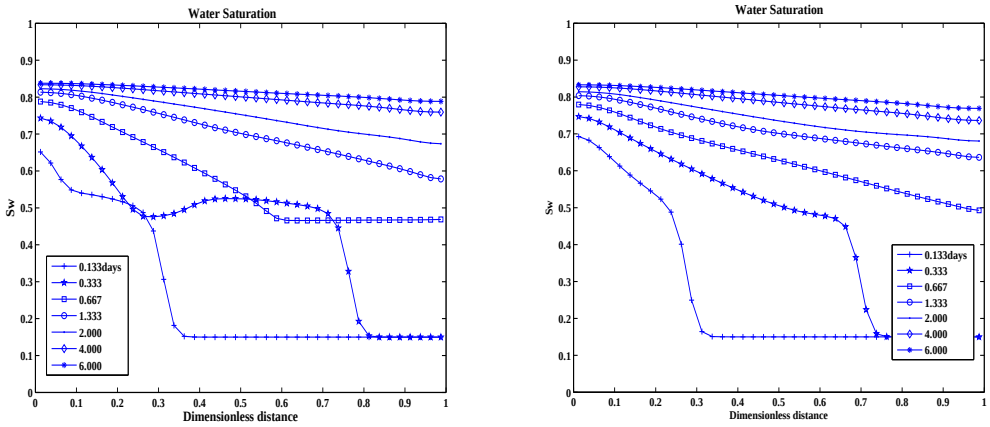

FIGURE 16. Plots showing the water saturation s along the core, for different invading sea water brines, at different times during a time period of 6 days. **Left**: SW2. **Right**: SW.

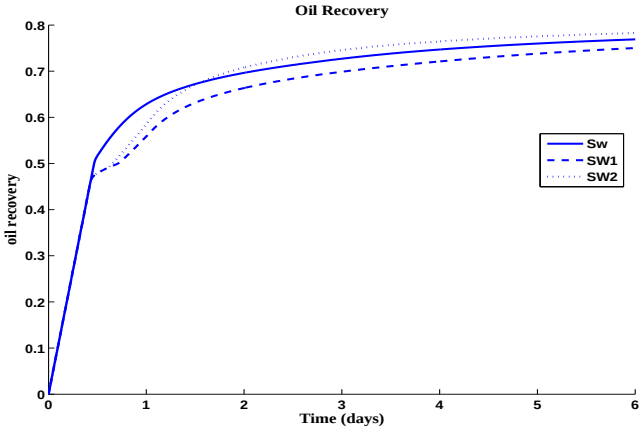

FIGURE 17. Oil recovery for different invading sea water brines. SW showing better recovery at early time after which SW2 performs better, due to a stronger release of Ca^{2+} ions from the rock, which in turn contributes to a change of wetting state.

steady state of the β_{ca}, β_{mg} and β_{na} is not reached for the duration of the example. Fig. 20 shows the concentrations of the different ions along the core at various times. As a consequence of the large adsorption of Ca^{2+} and Mg^{2+} ions on the rock surface, there exists certain regions along the core where the Ca^{2+} and Mg^{2+} concentrations are below the injected and initial concentrations. The Na^{+} ions are desorbed from the rock surface and this desorption is responsible for the Na^{+} concentration profile seen in Fig. 20. The Cl^{-} acts as a tracer and is neither desorbed or adsorbed.

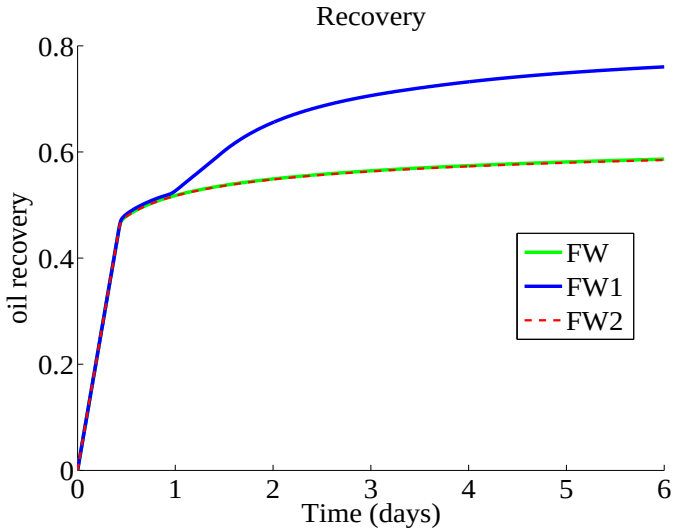

FIGURE 18. Oil recovery for different formation brines and LSW as the invading brine.

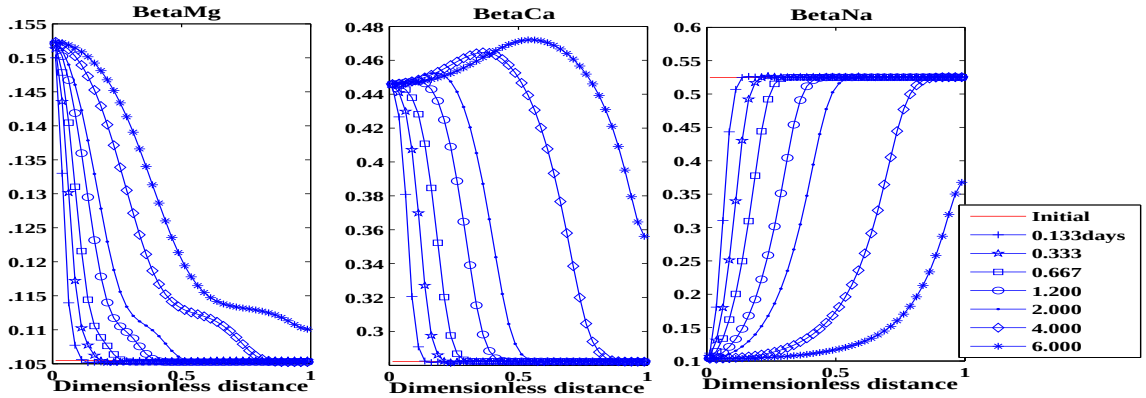

FIGURE 19. β-functions along the core for Example 3. **Left**: β_{mg}. **Middle**: β_{ca}. **Right**: β_{na}.

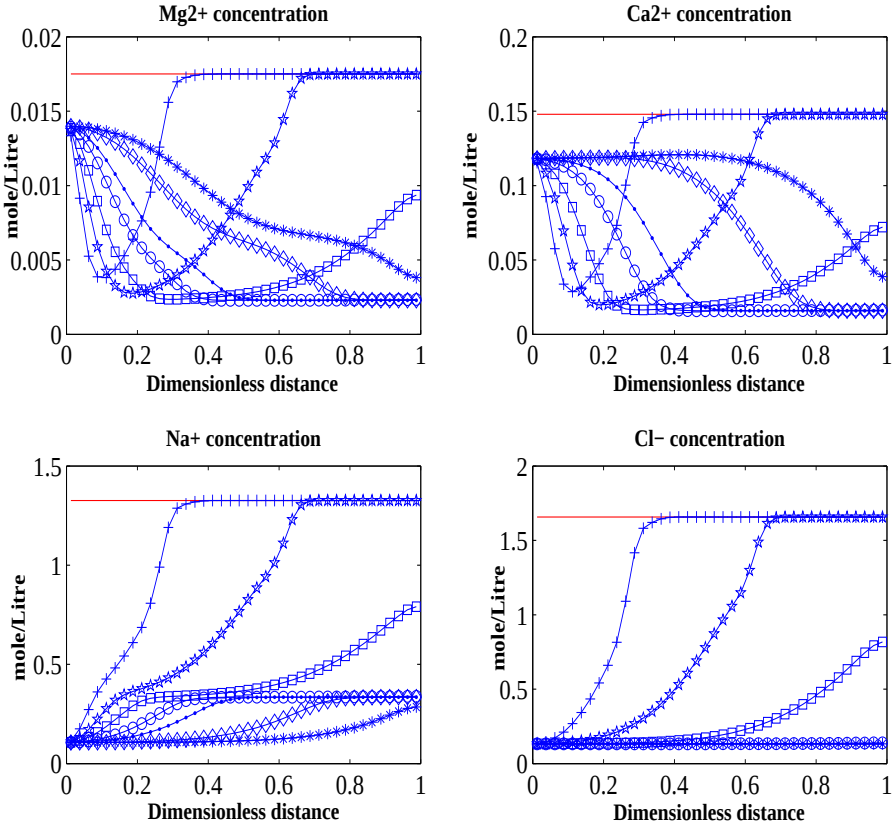

FIGURE 20. Concentrations along the core for Example 3. **Top Left**: Mg^{2+} concentration. **Top Right**: Ca^{2+} concentration. **Bottom Left**: Na^{+} concentration. **Bottom Right**: Cl^{-} concentration. Since the changes in the β_{mg} and β_{ca} concentrations seen in Fig. 19 now are of the same order as the concentrations of C_{mg} and C_{ca}, the interaction between them can clearly be observed. I.e., there is a "new" dip in the C_{mg} concentration front due to the strong adsorption of these ions to the rock as seen from the behavior of β_{mg}. Similarly for C_{ca} and C_{na}.

7. Concluding remarks

The proposed model which couples a standard Buckley-Leverett two-phase model to a multiple ion exchange process relevant for sandstone, and where desorption of divalent ions has been attributed a change of the wetting state such that more oil is mobilized, demonstrates how a range of different flow scenarios can occur. In particular, some main observations in view of the model behavior are:

- Different low salinity brines can give different degree of desorption of divalent ions (calcium and magnesium) from the rock surface, ranging from no desorption, partial desorption (either calcium or magnesium), or full desorption (both calcium and magnesium). This gives rise to different oil recovery curves ranging from no additional oil recovery effect to a more or less strong additional effect.
- Flooding with a seawater like brine and diluted variants of this gave rise to different degrees of calcium desorption, but no desorption of magnesium. It was observed that the speed of these desorption fronts were quite sensitive for the brine composition, leading to a range

of different oil recovery behavior in the initial stage (first 2 days) of the simulated flooding experiments.

- The model demonstrates that the oil recovery is quite sensitive to the composition of the formation water relative to the injected water composition.

In the future we will focus on expanding the model by including effects of e.g. capaillary pressure and mineral solubility, as well as evaluating the model by carrying out systematic comparison studies between predicted model behavior and different experimental works, as mentioned in the introduction part.

Acknowledgments

This research has been supported by the Norwegian Research Council, Statoil, Dong Energy, and GDF Suez, through the project Low Salinity Waterflooding of North Sea Sandstone Reservoirs. The second author is also supported by A/S Norske Shell

References

1. G. Ali, V. Furuholt, R. Natalini, and I. Torcicollo, *A mathematical model of sulphite chemical aggression of limestones with high permeability. part i. modeling and qualitative analysis*, Transport Porous Med **69** (2007), 109–122.
2. _____, *A mathematical model of sulphite chemical aggression of limestones with high permeability. part ii. numerical approximation*, Transport Porous Med **69** (2007), 175–188.
3. M. Alotaibi, R. Azmy, and H. Nasr-El-Din, *A comprehensive EOR study using low salinity water in sandstone reservoirs*, 17th Symposium on Improved Oil Recovery (Tulsa, Oklahoma, USA), SPE 129976, April 2010.
4. C.A.J. Appelo and D. Postma, *Geochemistry, groundwater and polution*, 2nd edition ed., CRC Press, 2005.
5. A. Ashraf, N. Hadia, and O. Torsæter, *Laboratory investigation of low salinity waterflooding as secondary recovery process: effect of wettability*, SPE Oil and Gas India Conference and Exhibition (Mumbai, India), SPE 129012, January 2010.
6. T. Austad, A. Rezaeidoust, and T. Puntervold, *Chemical mechanism of low salinity water flooding in sandstone reservoirs*, 17th Symposium on Improved Oil Recovery (Tulsa, Oklahoma, USA), SPE 129767, April 2010.
7. G.I. Barenblatt, V.M. Entov, and V.M. Ryzhik, *Theory of fluid flows through natural rocks*, Kluwer Academic Publisher, 1990.
8. J. Bear, *Dynamics of fluids in porous media*, Elsevier, Amsterdam, 1972.
9. S. Berg, A. Cense, E. Jansen, and K. Bakker, *Direct experimental evidence of wettability modification by low salinity*, International Symposium of the Society of Core Analyst (Noordwijk, The Netherlands), September 2009.
10. D. Boyd and K. Al Nayadi, *Validating laboratory measured archie saturation exponents using non-resistivity based methods*, International Symposium of the Society of Core Analyst (Abu Dhabi, UAE), October 2004.
11. Jui-Sheng Chen and Chen-Wuing Liu, *Numerical simulation of the evolution of aquifer porosity and species concentrations during reactive transport*, Computers & Geosciences **28** (2002), no. 4, 485 – 499.
12. Z. Chen, G. Huan, and Y. Ma, *Computational methods for multiphase flows in porous media*, Computational Science And Engineering, Society for Industrial and Applied Mathematics, 2006.
13. M. Cissokho, S. Boussour, P. Cordier, H. Bertin, and G. Hamon, *Low salinity oil recovery on clayey sandstone: experimental study*, International Symposium of the Society of Core Analyst (Noordwijk, The Netherlands), September 2009.
14. S. Evje and A. Hiorth, *A mathematical model for dynamic wettability alteration controlled by water-rock chemistry*, Networks and Heterogeneous Media **5** (2010), 217–256.
15. _____, *A model for interpretation of brine-dependent spontaneous imbibition experiments*, Advances in Water Resources **34** (2011), 1627–1642.
16. S. Evje, A. Hiorth, M.V. Madland, and R.Korsnes, *A mathematical model relevant for weakening of chalk reservoirs due to chemical reactions*, Networks and Heterogeneous Media **4** (2009), 755–788.
17. H. Helgeson, D. Kirkham, and G. Flowers, *Theoretical prediction of the thermodynamic behaviour of aqueous electrolytes by high pressure and temperatures; ii*, American Journal of Science **274** (1974), 1199–1261.
18. H. Helgeson, D. Kirkham, and G Flowers, *Theoretical prediction of the thermodynamic behaviour of aqueous electrolytes by high pressure and temperatures; iv*, American Journal of Science **281** (1981), 1249–1516.
19. A. Hiorth, L.M. Cathles, J. Kolnes, O. Vikane, A. Lohne, and Madland M.V., *A chemical model for the seawater-CO_2-carbonate system – aqueous and surface chemistry*, Wettability Conference (Abu Dhabi, UAE), October 2008.
20. G. Hirasaki, *Ion exchange with clays in the presence of surfactants*, SPE J. **22** (1982), 181–192.

21. P.P. Jadhunandan and N.R. Morrow, *Effect of wettability on waterflood recovery for crude oil/brine/rock systems.*, SPE Reservoir Engineering **12** (1995), 40–46.
22. G.R. Jerauld, C.Y. Lin, K.J. Webb, and J.C. Seccombe, *Modeling low-salinity waterflooding*, SPE Reservoir Evaluation & Engineering **11** (2008), 1000–1012.
23. S. Jin, Z. Xin, Shi Jin, and Zhouping Xin, *The relaxation schemes for systems of conservation laws in arbitrary space dimensions*, Comm. Pure Appl. Math **48** (1995), 235–277.
24. A. Lager, K. Webb, C. Black, M. Singleton, and K. Sorbie, *Low salinity oil recovery: An experimental investigation*, International Symposium of the Society of Core Analyst (Trondhiem, Norway), September 2006.
25. A.C. Lasaga, *Kinetic theory in the earth sciences*, Princeton series in geochemistry, Princeton University Press, 1998.
26. D.A. Nield and A. Bejan, *Convection in porous media*, Springer, 2006.
27. E.H. Oelkers and J. Schott, *Thermodynamics and kinetics of water-rock interaction*, Reviews in Mineralogy and Geochemistry, no. v. 70, Mineralogical Society of America, 2009.
28. A. Omekeh, S. Evje, I. Fjelde, and H.A. Friis, *Experimental and modeling investigation of ion exchange during low salinity waterflooding*, International Symposium of the Society of Core Analyst (Austin, Texas, USA), September 2011.
29. Adolfo P. Pires, Pavel G. Bedrikovetsky, and Alexander A. Shapiro, *A splitting technique for analytical modelling of two-phase multicomponent flow in porous media*, Journal of Petroleum Science and Engineering **51** (2006), no. 1 - 2, 54 – 67.
30. G.A. Pope, L.W. Lake, and F.G. Helfferich, *Cation exchange in chemical flooding: Part 1–basic theory without dispersion*, Society of Petroleum Engineers Journal **18** (1978), 418–434.
31. H. Pu, X. Xie, P. Yin, and N. Morrow, *Application of coalbed methane water to oil recovery by low salinity waterflooding*, SPE Improved Oil Recovery Symposium (Tulsa, Oklahoma, USA), SPE 113410, April 2008.
32. M. Sahimi, *Flow and transport in porous media and fractured rock: From classical methods to modern approaches*, John Wiley & Sons, 2011.
33. S.Boussour, M. Cissokho, P. Cordier, H. Bertin, and G. Hamon, *Oil recovery by low salinity brine injection: laboratory results outcrop and reservoir cores*, SPE Annual Technical Conference and Exhibition (New Orleans, USA), SPE 124277, October 2009.
34. J. Seccombe, A. Lager, K. Webb, G. Jerauld, and E. Fueg, *Improving waterflood recovery: LoSal EOR field evaluation*, SPE/DOE Symposium on Improved Oil Recovery (Tulsa, Oklahoma, USA), SPE 113480, April 2008.
35. M. Sharma and P. Filoco, *Effect of brine salinity and crude oil properties on oil recovery and residual saturations*, SPE Journal **5** (2000), 293–300.
36. K. Skrettingland, K. Holt, M. Tweheyo, and I. Skjevrak, *Snorre low salinity water injection - core flooding experiments and single well field pilot*, Symposium on Improved Oil Recovery (Tulsa, Oklahoma, USA), SPE 129877, April 2010.
37. Skule Strand, Eli J. Hagnesen, and Tor Austad, *Wettability alteration of carbonates- effects of potential determining ions (Ca^{2+} and SO_4^{2-}) and temperature*, Colloids and Surfaces A: Physicochemical and Engineering Aspects **275** (2006), no. 1-3, 1 – 10.
38. T.A.Dutra, A.P.Pires, and P.G.Bedrikovetsky, *A new splitting scheme and existence of elliptic region for gasflood modeling*, SPE J. **14** (2009), no. 1, 101–111.
39. G. Tang and N. Morrow, *Oil recovery by waterflooding and imbibition - invading brine cation valency and salinity*, International Symposium of the Society of Core Analysts (Golden, CO), August 1999.
40. Guo Qing Tang and Norman R Morrow, *Influence of brine composition and fines migration on crude oil/brine/rock interactions and oil recovery*, Journal of Petroleum Science and Engineering **24** (1999), no. 2-4, 99 – 111.
41. I. Tripathi and K.K. Mohanty, *Instability due to wettability alteration in displacements through porous media*, Chemical Engineering Science **63** (2008), no. 21, 5366 – 5374.
42. K. Webb, C. Black, and H. Al-Jeel, *Low salinity oil recovery - log inject log*, SPE/DOE Symposium on Improved Oil Recovery (Tulsa, Oklahoma, USA), SPE 89379, April 2004.

43. K. Webb, A. Lager, and C. Black, *Comparison of high/low salinity water/oil relative permeability*, International Symposium of the Society of Core Analysts (Abu Dhabi, UAE), November 2008.
44. Hasan O. Yildiz and Norman R. Morrow, *Effect of brine composition on recovery of moutray crude oil by waterflooding*, Journal of Petroleum Science and Engineering **14** (1996), no. 3-4, 159 – 168.
45. L. Yu, S. Evje, H. Kleppe, T. Kaarstad, I. Fjelde, and S.M. Skjaeveland, *Modelling of wettability alteration processes in carbonate oil reservoirs*, Networks and Heterogeneous Media **3** (2008), 149–183.
46. ———, *Spontaneous imbibition of seawater into preferentially oil-wet chalk cores : Experiments and simulations*, Journal of Petroleum Science and Engineering **66** (2009), no. 3-4, 171 – 179.
47. W. Yu-shu and B. Baojun, *Efficient simulstion for low salinity waterflooding in porous and fractured reservoirs*, SPE Reservoir Simulation Symposium (The Woodlands, Texas, USA), SPE 118830, February 2009.
48. Y. Zhang and N. Morrow, *Comparison of secondary and tertiary recovery with change in injection brine composition for crude oil/sandstone combinations*, SPE/DOE Symposium on Improved Oil Recovery (Tulsa, Oklahoma, USA), SPE 99757, April 2006.

8. APPENDIX A: DATA FOR WATER-ROCK CHEMISTRY

Activity coefficients. Along the line of the previous work [16] the following values, taken from [4], are used for the constants a_i^0:

$$a_{ca}^0 = 5, \quad a_{na}^0 = 4, \quad a_{cl}^0 = 3.5, \quad a_{mg}^0 = 5.5, \quad a_{so}^0 = 5. \tag{94}$$

and for b_i^0 we use:

$$b_{ca}^0 = 0.165, \quad b_{na}^0 = 0.075, \quad b_{cl}^0 = 0.015, \quad b_{mg}^0 = 0.2, \quad b_{so}^0 = -0.04. \tag{95}$$

Moreover, we shall use the following values for $A(T)$ and $B(T)$ taken from [18, 17]:

$$A(T = 80) = 0.5706, \qquad B(T = 80) = 0.3381. \tag{96}$$

Core properties. The following core properties are assumed for the model example studied below.

- Length: $L = 0.04\,\mathrm{m}$
- Porosity: $\phi = 0.274$
- Mass of clay: $M_c = 0.088\,\mathrm{Kg/Litre\ of\ core}$
- Permeability: $\kappa = 500\,\mathrm{mD} = 500 \cdot 0.987 \cdot 10^{-15}\,\mathrm{m}^2$.

Oil and brine properties.

- Oil viscosity: $\mu_o = 0.6$ cp (1 cp $= 10^{-3}$ Pa s)
- Water viscosity: $\mu = 0.3$ cp

Properties connected to the cation exchange process.

- Cation exchange capacity: $CEC = 0.013\,\mathrm{eq/Kg\ of\ clay}$
- Selectivity factor : $K_{cana}^{HS} = 5.1$; $K_{cana}^{LS} = 1.7$
- Selectivity factor: $K_{mgna}^{HS} = 4.8$; $K_{mgna}^{LS} = 1.6$
- Corresponding brine salinity : $B_s^{HS} = 4.5$; $B_s^{LS} = 10^{-8}$
- r constant $r = 400$.

Other quantities.

- Total velocity $v_T = 0.01$ m/day$= 1.1574 \cdot 10^{-7}$ m/s.
- Reference diffusion coefficient: $\overline{D}_m = Lv_T = 4.6296 \cdot 10^{-9}\ \mathrm{m}^2/\mathrm{s} \approx 5 \cdot 10^{-9}\ \mathrm{m}^2/\mathrm{s}$.
- Reference viscosity: $\overline{\mu} = 10^{-3}$ Pa s.

The molecular diffusion coefficient D_m is set equal to reference diffusion $\overline{D}_m$. Since the total velocity v_T is low and the dispersion length α of the order of millimeters, the Peclet number (33) becomes small (< 1), and the first term of (32) only is used. In addition, for all simulations we have used the choice $p = q = 1.9$ in the expression for molecular diffusion given by equation (32). Oil recovery is defined as

$$\text{Oil Recovery} := \frac{\int_0^1 [s(x,t) - s_{\text{init}}(x)]\, dx}{\int_0^1 [1 - s_{\text{init}}(x)]\, dx},$$

where $s_{\text{init}}(x)$ is initial water saturation in the core.

Ions	FW [mol/l]	LSW [mol/l]	LSW1 [mol/l]	LSW2 [mol/l]	LSW3 [mol/l]
Na^+	1.3262	0.013262	0.13262	0.13262	0.13262
Cl^-	1.6569	0.016570	0.17050	0.13907	0.13266
Ca^{2+}	0.1479	0.001479	0.00148	0.00148	0.00001
Mg^{2+}	0.0175	0.000175	0.01746	0.00175	0.00001
SO_4^{2-}	0.0000	0.000000	0.00000	0.00000	0.00000
Ion Strength I_0	1.8224	0.018224	0.18944	0.17373	0.13616

TABLE 1. Composition of the formation water and the different brines used for Example 1, Case 1.

Ions	FW [mol/l]	SW [mol/l]	SW1 [mol/l]	SW2 [mol/l]
Na^+	1.3262	0.45014	0.045014	0.045014
Cl^-	1.6569	0.51912	0.051912	0.049316
Ca^{2+}	0.1479	0.01299	0.001299	0.000001
Mg^{2+}	0.0175	0.04551	0.004551	0.004551
SO_4^{2-}	0.0000	0.02401	0.002401	0.002401
Ion Strength I_0	1.8224	0.64965	0.064965	0.061071

TABLE 2. Composition of the formation water and the different brines used for Example 1, Case 2.

Ions	LSW [mol/l]	FW [mol/l]	FW1 [mol/l]	FW2 [mol/l]
Na^+	0.013262	1.3262	1.3262	0.45014
Cl^-	0.016570	1.6569	1.9712	0.51912
Ca^{2+}	0.001479	0.1479	0.1479	0.01299
Mg^{2+}	0.000175	0.0175	0.1746	0.04551
SO_4^{2-}	0.000000	0.0000	0.0000	0.02401
Ion Strength I_0	0.018224	1.8224	2.2937	0.64965

TABLE 3. Composition of the brine and the different formation waters used for Example 2.

Ions	FW [mol/l]	IW [mol/l]
Na^+	1.3262	1.0610
Cl^-	1.6569	1.3255
Ca^{2+}	0.1479	0.1183
Mg^{2+}	0.0175	0.0140
SO_4^{2-}	0.0000	0.0000
Ion Strength I_0	1.8224	1.4578

TABLE 4. Composition of the formation water and the different brines used for Example 3.

APPENDIX B: DATA FOR WATER-OIL FLOW FUNCTIONS

High salinity conditions. The following set of values for *oil-wet* conditions is used:

$$k^{*,ow} = 0.3,\ k_o^{*,ow} = 0.75,\ \ s_{wr}^{ow} = 0.15,\ \ s_{or}^{ow} = 0.3,\ \ Nk^{ow} = 3, \quad Nk_o^{ow} = 2. \tag{97}$$

Applying these values in (14) the following two relative permeability curves are obtained

$$k^{ow}(s; s_{wr}^{ow}, s_{or}^{ow}), \qquad k_o^{ow}(s; s_{wr}^{ow}, s_{or}^{ow}), \qquad \text{for } s_{wr}^{ow} \le s \le 1 - s_{or}^{ow}.$$

Low salinity conditions. The following set of values for *water-wet* conditions is used:

$$k^{*,ww} = 0.4,\ k_o^{*,ww} = 0.9,\ \ s_{wr}^{ww} = 0.15,\ \ s_{or}^{ww} = 0.15,\ \ Nk^{ww} = 3,\ \ Nk_o^{ww} = 2. \tag{98}$$

These choices give corresponding relative permeability curves

$$k^{ww}(s; s_{wr}^{ww}, s_{or}^{ww}), \quad k_o^{ww}(s; s_{wr}^{ww}, s_{or}^{ww}), \quad \text{for } s_{wr}^{ww} \le s \le 1 - s_{or}^{ww}.$$

International Research Institute of Stavanger, P.O.Box 8046, 4068 Stavanger, Norway.
E-mail: Aruoture.Voke.Omekeh@iris.no

University of Stavanger (UiS), 4036 Stavanger, Norway.
E-mail: Steinar.Evje@uis.no

International Research Institute of Stavanger, P.O.Box 8046, 4068 Stavanger, Norway.
E-mail: HelmerAndre.Friis@iris.no